Available online at www.sciencedirect.com
ScienceDirect
Cement and Concrete Research 38 (2008) 137–158
Cement and Concrete Research

# The calcium silicate hydrates

I.G. Richardson*

*School of Civil Engineering, University of Leeds, Leeds LS2 9JT, United Kingdom*

Received 16 November 2007; accepted 19 November 2007

**Abstract**

This article is concerned with the calcium silicate hydrates, including crystalline minerals and the extremely variable and poorly ordered phase (C-S-H) that is the main binding phase in most concrete. Up-to-date composition and crystal-structure information is tabulated for the most important crystalline calcium (alumino) silicate hydrates and related phases. A number of models for the nanostructure of C-S-H are summarized and compared and it is shown that there is much more of a consensus than might seem apparent at first sight. The value of the recently solved structures of 1.4 nm tobermorite and jennite, together with those of jaffeite and metajennite, for visualizing the nanostructural elements present in the models is demonstrated. The importance of Hal Taylor's contribution to the solution of the structure of jennite is highlighted. The applicability of Richardson and Groves' model is demonstrated using experimental composition-structure observations on the nature of C-S-H in a Portland cement-fly ash blend.


*Keywords:* Cement; Calcium silicate hydrate (C-S-H); Crystal structure; TEM

## 1. Introduction

Many naturally occurring crystalline calcium silicate hydrates or calcium aluminosilicate hydrates are relevant to Cement Science, either because they are formed hydrothermally — as in deep oil-well or geothermal cements — or in autoclaved or hot-pressed materials, or because their structures have proved to be very useful in modeling the structure of the extremely variable and poorly ordered phase that is essentially the 'glue' of the concrete part of the Built Environment. The nature of this phase was discussed [1–3] at the meeting in London in 1918 that later came to be considered to be the first in the series of international conferences on the chemistry of cement of which this is the twelfth.[1] In the opening sentence to the first paper read at that meeting in 1918, Cecil H. Desch noted with regard to calcareous cements that '*…our knowledge of the scientific nature of the materials and processes involved is even yet imperfect, in spite of many excellent investigations covering various parts of the subject*'. The same statement could be used today, but ninety additional years of investigations — utilizing increasingly sophisticated experimental techniques — have of course resulted in many significant advances in our knowledge; the Proceedings of the international conferences in this series have to date been a valuable record of those advances, as is outlined by Francis Young elsewhere in this issue [4]. The purpose of this article is threefold: firstly, to tabulate up-to-date composition and crystal-structure information for the most important calcium (alumino) silicate hydrates and related phases, which should be a useful reference source for others interested in these phases; secondly, to summarize and compare the various models that exist for the nanostructure of the calcium silicate hydrate (C-S-H) phase in hardened $C_3S$ and Portland cements — or in blends of Portland cement with supplementary cementing materials —many of which are in fact much more similar to one another than might seem apparent at first sight; and thirdly, to highlight the recent solutions to the structures of jaffeite, jennite, metajennite (as yet unrefined) and 1.4 nm tobermorite, and to demonstrate how the structures of these phases are useful for

* Tel.: +44 113 343 2331; fax: +44 113 343 2265.
*E-mail address:* I.G.Richardson@leeds.ac.uk.

[1] The meeting of the Faraday Society to discuss 'The Setting and Hardening of Cements and Plasters' was held on Monday, January 14, 1918, in the House of the Royal Society of Arts, John Street, Adelphi, London, and was published in Volume 14 of the Transactions of the Faraday Society in January 1919. The Faraday Society '*...had intended to inaugurate a research into the question of cements and setting generally, realizing its great importance, but there has been great difficulty in this owing to the war, and the Council have considered the best thing they can do is to have a discussion such as we are going to have this evening*' (James Swinburne FRS, Past-President and Chair of the meeting).

0008-8846/$ - see front matter © 2007 Elsevier Ltd. All rights reserved.
doi:10.1016/j.cemconres.2007.11.005

Table 1
Crystal-structure data for calcium silicate hydrates, calcium aluminosilicate hydrates and related phases

| Name | Formula | Ca/Si | References | Sy | SG | $M_r$ cell g mol$^{-1}$ | $Z$ | $M_r$ formula g mol$^{-1}$ | $V$ Å$^3$ | $D_c$ g cm$^{-3}$ | $a$ Å | $b$ | $c$ | $\alpha$ | $\beta$ | $\gamma$ |
|---|---|---|---|---|---|---|---|---|---|---|---|---|---|---|---|---|
| *(a). Wollastonite group* | | | | | | | | | | | | | | | | |
| Foshagite | $Ca_4(Si_3O_9)(OH)_2$ | 1.33 | [6,7,8,**9,10**] | Tc | $P\bar{1}$ | 845.17 | 2 | 422.59 | 513.0 | 2.736 | 10.32 | 7.36 | 7.04 | 90 | 106.4 | 90 |
| Hillebrandite | $Ca_2(SiO_3)(OH)_2$ | 2.00 | [11,12,**9,10,13–17**] | O | *C m c* $2_1$ | 1141.53 | 6 | 190.25 | 702.1 | 2.700 | 3.6389 | 16.311 | 11.829 | 90 | 90 | 90 |
| Nekoite | $Ca_3Si_6O_{15}\cdot 7H_2O$ | 0.50 | [18,19–21] | Tc | *P*1 | 654.85 | 1 | 654.85 | 490.3 | 2.217 | 7.588 | 9.793 | 7.339 | 111.77 | 103.5 | 86.53 |
| Okenite | $[Ca_8(Si_6O_{16})(Si_6O_{15})_2(H_2O)_6]^{4-}[Ca_2(H_2O)_9\cdot 3H_2O]^{4+}$ | 0.56 | [22,23,**10,16**] | Tc | $P\bar{1}$ | 1966.60 | 1 | 1966.60 | 1418.5 | 2.302 | 9.69 | 7.28 | 22.02 | 92.7 | 100.1 | 110.9 |
| Pectolite | $Ca_2NaHSi_3O_9$ | 1.00 [a] | [24,25–29,**30**] | Tc | $P\bar{1}$ | 664.821 | 2 | 332.41 | 382.2 | 2.888 | 7.98 | 7.023 | 7.018 | 90.54 | 95.14 | 102.55 |
| Wollastonite 1A | $Ca_3Si_3O_9$ | 1.00 | [31,29,32,33,**13,34**] | Tc | $P\bar{1}$ | 696.98 | 2 | 348.49 | 396.96 | 2.916 | 7.9258 | 7.3202 | 7.0653 | 90.055 | 95.217 | 103.43 |
| Xonotlite [b] | $Ca_6Si_6O_{17}(OH)_2$ | 1.00 | [35,36,**10,13,14,37–45**] | M | *P* 1 2/*a* 1 | 1427.99 | 2 | 713.99 | 879.3 | 2.700 | 17.032 | 7.363 | 7.012 | 90 | 90.36 | 90 |
| *(b). Tobermorite group* | | | | | | | | | | | | | | | | |
| Clinotobermorite [c] | $Ca_5Si_6O_{17}\cdot 5H_2O$ | 0.83 | [46,47,48–50,45,**51**] | M | *C 1 c 1* | 2923.93 | 4 | 730.98 | 1859.64 | 2.611 | 11.276 | 7.343 | 22.642 | 90 | 97.28 | 90 |
| Clinotobermorite [d] | $Ca_5Si_6O_{17}\cdot 5H_2O$ | 0.83 | | Tc | *C 1* | 1461.97 | 2 | 730.98 | 929.8 | 2.611 | 11.274 | 7.344 | 11.468 | 99.18 | 97.19 | 90.03 |
| 'Clinotobermorite 9 Å' [c] | $Ca_5Si_6O_{16}(OH)_2$ | 0.83 | [46,47,**51**] | M | *C 12/ c 1* | 2635.68 | 4 | 658.92 | 1528.03 | 2.864 | 11.161 | 7.303 | 18.771 | 90 | 92.91 | 90 |
| 'Clinotobermorite 9 Å' [d] | $Ca_5Si_6O_{16}(OH)_2$ | 0.83 | | Tc | $C\bar{1}$ | 1317.84 | 2 | 658.92 | 763.9 | 2.865 | 11.156 | 7.303 | 9.566 | 101.08 | 92.83 | 89.98 |
| Oyelite | $Ca_{10}B_2Si_8O_{29}\cdot 12.5H_2O$ | 1.25 | [52,53] | O | n.d. | 2672.52 | 2 | 1336.26 | 1668.77 | 2.659 | 11.25 | 7.25 | 20.46 | 90 | 90 | 90 |
| 9 Å tobermorite (riversideite) [c] | $Ca_5Si_6O_{16}(OH)_2$ | 0.83 | [**51**,54,55] | O | *F d* 2 *d* | 5271.37 | 8 | 658.92 | 3055.25 | 2.865 | 11.16 | 7.32 | 37.40 | 90 | 90 | 90 |
| 9 Å tobermorite (riversideite) [d] | $Ca_5Si_6O_{16}(OH)_2$ | 0.83 | | M | *P* 1 1 $2_1/a$ | 1317.84 | 2 | 658.92 | 764.78 | 2.861 | 6.7 | 7.32 | 18.70 | 90 | 90 | 123.5 |
| Anomalous 11 Å tobermorite [c] | $Ca_4Si_6O_{15}(OH)_2\cdot 5H_2O$ | 0.67 | [50,56,50,54] | O | *F 2 d d* | 5543.35 | 8 | 692.92 | 3741.65 | 2.460 | 11.265 | 7.386 | 44.970 | 90 | 90 | 90 |
| Anomalous 11 Å tobermorite [d] | $Ca_4Si_6O_{15}(OH)_2\cdot 5H_2O$ | 0.67 | [56–60,**9,10,14**] | M | *B 1 1 m* | 1385.84 | 2 | 692.92 | 935.4 | 2.460 | 6.735 | 7.385 | 22.487 | 90 | 90 | 123.25 |
| Normal 11 Å tobermorite [d] | $Ca_{4.5}Si_6O_{16}(OH)\cdot 5H_2O$ | 0.75 | [**34,41,44,45,51,61–65**] | M | *B 1 1 m* | 1423.88 | 2 | 711.94 | 941.68 | 2.460 | 6.732 | 7.369 | 22.680 | 90 | 90 | 123.18 |
| 14Å tobermorite (plombierite) [c] | $Ca_5Si_6O_{16}(OH)_2\cdot 7H_2O$ | 0.83 | [66,67–69] | O | *F 2 d d* | 6280.23 | 8 | 785.03 | 4578.56 | 2.278 | 11.2 | 7.3 | 56.0 | 90 | 90 | 90 |
| 14Å tobermorite (plombierite) [d] | $Ca_5Si_6O_{16}(OH)_2\cdot 7H_2O$ | 0.83 | [**44,51,63**] | M | *B 1 1 b* | 1570.06 | 2 | 785.03 | 1170.4 | 2.228 | 6.735 | 7.425 | 27.987 | 90 | 90 | 123.25 |
| *(c). Jennite group* | | | | | | | | | | | | | | | | |
| Jennite | $Ca_9Si_6O_{18}(OH)_6\cdot 8H_2O$ | 1.50 | [70,60,71–74,**12**] | Tc | $P\bar{1}$ | 1063.44 | 1 | 1063.44 | 759.5 | 2.325 | 10.576 | 7.265 | 10.931 | 101.30 | 96.98 | 109.65 |
| Metajennite | $Ca_9Si_6O_{18}(OH)_6\cdot 8H_2O$ | 1.50 | [75,70,72] | M | I 1 2/*m* 1 | 955.30 | 1 | 955.30 | 631.1 | 2.513 | 9.944 | 3.638 | 17.72 | 90 | 100.09 | 90 |

| | | | | | | | | | | | | | | | | |
|---|---|---|---|---|---|---|---|---|---|---|---|---|---|---|---|---|
| *(d). Gyrolite Group* | | | | | | | | | | | | | | | | |
| Fedorite | $(Na,K)_2(Ca,Na)_7(Si,Al)_{16}O_{38}(F,OH)_2{\cdot}3.5H_2O$ [f] | 0.56 [e] | [76,77,**51**] | Tc | $P\bar{1}$ | 1448.66 | 1 | 1448.66 | 961.24 | 2.503 | 9.645 | 9.6498 | 12.617 | 102.43 | 96.247 | 119.89 |
| Gyrolite | $NaCa_{16}Si_{23}AlO_{60}(OH)_8{\cdot}14H_2O$ | 0.71 [e] | [78,79–81,**9,10,16, 30,38,41–43,51,82,83**] | Tc | $P\bar{1}$ | 2685.47 | 1 | 2685.47 | 1824.1 | 2.445 | 9.74 | 9.74 | 22.40 | 95.7 | 91.5 | 120 |
| K-phase | $Ca_7Si_{16}O_{38}(OH)_2$ | 0.44 | [**51,9**] | Tc | $P\bar{1}$ | 1371.91 | 1 | 1371.91 | 944.39 | 2.412 | 9.70 | 9.70 | 12.25 | 101.9 | 96.5 | 120 |
| Reyerite | $Na_2Ca_{14}Si_{22}Al_2O_{58}(OH)_8{\cdot}6H_2O$ | 0.67 [e] | [84,80,81,85,86,**51**] | Tg | $P\bar{3}$ | 2451.07 | 1 | 2451.07 | 1574.6 | 2.585 | 9.765 | 9.765 | 19.067 | 90 | 90 | 120 |
| Truscottite | $Ca_{14}Si_{24}O_{58}(OH)_8{\cdot}2H_2O$ | 0.58 | [81,87,88,**9,43,51**] | Tg | $P\bar{3}$ | 2335.20 | 1 | 2335.20 | 1545.5 | 2.509 | 9.735 | 9.735 | 18.83 | 90 | 90 | 120 |
| Z-phase | $Ca_9Si_{16}O_{40}(OH)_2{\cdot}14H_2O$ | 0.56 | [78,81,**42,51,82**] | Tc | $P\bar{1}$ | 1736.27 | 1 | 1736.27 | 1238.3 | 2.328 | 9.70 | 9.70 | 15.24 | 90.94 | 93.19 | 120 |
| *(e). $\gamma$-$C_2S$ group* | | | | | | | | | | | | | | | | |
| Calcium chondrodite [g] | $Ca_5[SiO_4]_2(OH)_2$ | 2.50 | [89, 90–93,**15,17**] | M | $P\,1\,1\,2_1/b$ | 837.16 | 2 | 418.58 | 492.1 | 2.825 | 8.9207 | 11.4481 | 5.0759 | 90 | 90 | 108.32 |
| Kilchoanite | $Ca_6(SiO_4)(Si_3O_{10})$ | 1.50 | [94,9,17,40] | O | $I\,2\,c\,m$ | 2307.21 | 4 | 576.80 | 1275.9 | 3.003 | 11.42 | 5.09 | 21.95 | 90 | 90 | 90 |
| *(f). Other calcium silicate phases* | | | | | | | | | | | | | | | | |
| Afwillite | $Ca_3(SiO_3OH)_2{\cdot}2H_2O$ | 1.50 | [95,96–100,**9, 10,14,44,64**] | M | $C\,1\,c\,1$ | 1369.82 | 4 | 342.46 | 859.6 | 2.646 | 16.278 | 5.6321 | 13.236 | 90 | 134.90 | 90 |
| $\alpha$-$C_2SH$ | $Ca_2(HSiO_4)(OH)$ | 2.00 | [101,102,103,**9,13, 15,17,38,40,42,43,104**] | O | $P\,2_1/b\,2_1/c\,2_1/a$ | 1522.07 | 8 | 190.26 | 928.8 | 2.721 | 9.487 | 9.179 | 10.666 | 90 | 90 | 90 |
| Cuspidine [h] | $Ca_4(F_{1.5}(OH)_{0.5})Si_2O_7$ | 2.00 | [105,106–108,**13**] | M | $P\,1\,2_1/c\,1$ | 1461.96 | 4 | 365.49 | 814.2 | 2.982 | 7.518 | 10.521 | 10.906 | 90 | 70.7 | 90 |
| Dellaite | $Ca_6(Si_2O_7)(SiO_4)(OH)_2$ | 2.00 | [109,110,111,**15,17**] | Tc | $P\bar{1}$ | 1069.49 | 2 | 534.74 | 598.8 | 2.966 | 6.825 | 6.931 | 12.907 | 90.68 | 97.57 | 98.18 |
| Jaffeite | $Ca_6[Si_2O_7](OH)_6$ | 3.00 | [112,113,**15,17,38, 40,41,70,104**] | Tg | $P\,3$ | 1021.38 | 2 | 510.69 | 654.0 | 2.593 | 10.035 | 10.035 | 7.499 | 90 | 90 | 120 |
| Killalaite | $Ca_{6.4}(H_{0.6}Si_2O_7)_2(OH)_2$ | 1.60 | [114,115] | M | $P\,1\,2_1/m\,1$ | 1258.49 | 2 | 629.24 | 710.2 | 2.943 | 6.807 | 15.459 | 6.811 | 90 | 97.76 | 90 |
| Poldervaartite [i] | $Ca(Ca_{0.67}Mn_{0.33})(HSiO_4)(OH)$ | 2.00[j] | [116] | O | $P\,2_1/b\,2_1/c\,2_1/a$ | 1561.69 | 8 | 195.21 | 904.8 | 2.866 | 9.398 | 9.139 | 10.535 | 90 | 90 | 90 |
| Rosenhahnite | $Ca_3Si_3O_8(OH)_2$ | 1.00 | [117,118–120] | Tc | $P\bar{1}$ | 733.02 | 2 | 366.51 | 420.2 | 2.897 | 6.955 | 9.484 | 6.812 | 108.64 | 94.84 | 95.89 |
| Suolunite | $CaSiO_{2.5}(OH)_{\cdot 0.5}H_2O$ | 1.00 | [121,122–125] | O | $F\,d\,2\,d$ | 2146.87 | 16 | 134.18 | 1317.1 | 2.707 | 19.776 | 5.99 | 11.119 | 90 | 90 | 90 |
| Tilleyite | $Ca_5Si_2O_7(CO_3)_2$ | 2.50 | [126,**127,128**] | M | $P\,1\,2/a\,1$ | 1954.35 | 4 | 488.59 | 1131.8 | 2.867 | 15.108 | 10.241 | 7.579 | 90 | 105.17 | 90 |

*(continued on next page)*

Table 1 (*continued*)

| Name | Formula | Ca/Si | References | Sy | SG | $M_r$ cell g mol$^{-1}$ | $Z$ | $M_r$ formula g mol$^{-1}$ | $V$ Å$^3$ | $D_c$ g cm$^{-3}$ | $a$ Å | $b$ | $c$ | $\alpha$ | $\beta$ | $\gamma$ |
|---|---|---|---|---|---|---|---|---|---|---|---|---|---|---|---|---|
| *(g). Other high temperature cement phases* | | | | | | | | | | | | | | | | |
| Bicchulite | $Ca_2(Al_2SiO_6)(OH)_2$ | 0.67[k] | [129,130,131,**132**] | C | $I\bar{4}3m$ | 1168.86 | 4 | 292.22 | 688.9 | 2.818 | 8.8318 | 8.8318 | 8.8318 | 90 | 90 | 90 |
| Fukalite | $Ca_4(Si_2O_6)(CO_3)(OH)_2$ | 2.00 | [133,134] | O | $P\,2_1\,2_1\,2_1$ | 1626.02 | 4 | 406.50 | 966.2 | 2.794 | 3.786 | 10.916 | 23.379 | 90 | 90 | 90 |
| Katoite Hydrogarnet[l] | $Ca_{1.46}AlSi_{0.55}O_6H_{3.78}$ | 0.94[k] | [135,**38,41,65, 136–139**] | C | $I4_1/a\bar{3}2/d$ | 3211.72 | 16 | 200.73 | 1847.3 | 2.887 | 12.27 | 12.27 | 12.27 | 90 | 90 | 90 |
| Rustumite | $Ca_{10}(Si_2O_7)_2(SiO_4)Cl_2(OH)_2$ | 2.00 | [140,110] | M | $C\,1\,2/c\,1$ | 3736.56 | 4 | 934.14 | 2124.1 | 2.921 | 7.620 | 18.550 | 15.510 | 90 | 104.33 | 90 |
| Scawtite[m] | $Ca_7(Si_6O_{18})(CO_3)\cdot 2H_2O$ | 1.17 | [141,142–146,**13,127**] | M | $C\,1\,m\,1$ | 1666.21 | 2 | 833.11 | 1003.2 | 2.758 | 11.0394 | 15.1935 | 6.6344 | 90 | 115.645 | 90 |
| Strätlingite | $Ca_2Al(AlSi)_{2.22}O_2(OH)_{12}\cdot 2.25H_2O$ | 0.62[k] | [147,148–150,**151,152**] | Tg | $R\bar{3}2/m$ | 1334.65 | 3 | 444.88 | 1079.6 | 2.053 | 5.745 | 5.745 | 37.77 | 90 | 90 | 120 |

References for data that are associated with a full crystal-structure solution are shown underlined; other selected relevant references are included (not underlined), with those published since the 11th International Congress on the Chemistry of Cement shown in **bold** type. The crystal system (Sy) is indicated by: C = cubic; M = monoclinic; O = orthorhombic; Tg = trigonal; Tc = triclinic. SG = full international space group. $D_c$ is the calculated density.

[a] (Na+Ca)/Si.

[b] Ma2bc polytype (an $MDO_2$ polytype).

[c] $MDO_1$ polytype.

[d] $MDO_2$ polytype.

[e] (Na+K+Ca)/(Al+Si).

[f] Actual composition: $(Na_{1.29}\,K_{0.79})(Ca_{4.48}Na_{2.52})Si_{16}O_{38}F_2\cdot 3.47H_2O$.

[g] Synthetic phase similar to the mineral reinhardbraunsite, $Ca_5[SiO_4]_2(OH,F)_2$.

[h] Cuspidine: cell parameters given in the paper transformed by the following matrix (00-1/010/100).

[i] Isostructural with α-$C_2SH$; [j](Ca+Mn)/Si.

[k] Ca/(Si+Al).

[l] Composition is variable.

[m] Scawtite: cell parameter, *a*, given in the paper as 10.0394 is a mistake and has been corrected to 11.0394 Å.

visualizing the models for the nanostructure of C-S-H. The material in this article is extended in a companion paper [5] in which the cohesion forces that act between individual C-S-H layers or crystallites are considered, and two possible strategies are discussed for tuning the mechanical properties of cementitious materials based on modifying the bonding scheme in C-S-H.

## 2. Crystalline calcium silicate hydrates

Crystal-structure data are given in Table 1 for the most important calcium (alumino) silicate hydrates and related phases. The references for the data that are associated with full crystal-structure solutions are shown underlined; a selection of other relevant references are included (not underlined), with those published since the 11th International Congress on the Chemistry of Cement (ICCC) are shown in **bold** type. The arrangement of the phases in the table is derived from Table II of Taylor and Roy [153], which was the Principal Report at the 7th ICCC on the Structure and Composition of Hydrates. Whilst the information in Table 1 is much more comprehensive than that given by Taylor and Roy — and also more so than that given in a Plenary Paper at the 5th ICCC [154] — in contrast with those papers, no further discussion is provided in this article on the nature of the phases other than 1.4 nm tobermorite, jennite, metajennite and jaffeite. The reader is instead directed to the extensive list of references, which includes an excellent review article by Bonaccorsi and Merlino [51] in which the tobermorite and gyrolite groups are discussed in detail; Bonaccorsi and Merlino's determinations of the crystal structures of 1.4 nm tobermorite and jennite are two of the most significant advances in Cement Science since the 11th ICCC. Table 1 is intended to be a useful reference point for anybody interested in crystalline calcium silicate hydrates. In particular, the fact that the crystal structures have now been solved for so many of the phases means that calculated X-ray diffraction (XRD) patterns can be used instead of experimentally-derived patterns, which should enable more reliable indexing, checking of peak intensities and easier recognition of peaks from impurities.

## 3. Models for the nanostructure of C-S-H in hardened $C_3S$ and Portland cements, or in blends of Portland cement with supplementary cementing materials

Unfortunately, in contrast to the phases in Table 1, the C-S-H that is the principal binding phase in most concrete is nearly amorphous, and so X-ray diffraction techniques are of limited value. Any model that is developed for its nanostructure must of course be consistent with experimental observations from other techniques; most importantly, it must be compatible with the wide ranges in chemical composition and silicate (or aluminosilicate) anion structure that have been observed. The C-S-H present in hardened pastes of $C_3S$ or neat Portland cements generally has a mean Ca/Si ratio of about 1.75, with a range of values within a given paste from around 1.2 to 2.1 [155]; if a paste contains a supplementary cementing material — such as silica fume, fly ash, metakaolin or ground granulated blast-furnace slag — then the mean value is much reduced, in some cases to less than 1 [155]. In neat $C_3S$ or Portland cement pastes, the silicate anions vary in mean length from 2 in young pastes, to about 5 in mature pastes, whilst values of 20 or greater can be found in blended cements cured at elevated temperature (for example [156] ). As well as the mean length, a successful model must also account for the experimentally observed sequence of chain lengths; i.e. 2, 5, 8, … $(3n-1)$ where $n$ is integer (for individual structural units), and that in Al-substituted C-S-H, $Al^{3+}$ substitutes for $Si^{4+}$ only in the central tetrahedron of pentamers — or in every third tetrahedron in longer chains — which has now been observed by a number of workers [157–159]. It should also be remembered that there is some hydrated monomer to consider that forms during the induction period, some of which persists over long timescales (years) in some systems [160–162].

Unsurprisingly, given the importance of concrete to the Built Environment, a large number of models have been proposed for the nanostructure of C-S-H, many of which are listed in Table 2. Table 2 includes information on: the authors of each model; the principal reference(s) with date(s) of publication; the main crystalline phase from which the model is derived; the nature of the silicate anions; if given, the main formulation or structure-composition relationship; and some comments, including a brief note of links with other models. It is evident from the table that all the models fall into one of two categories: one where the silicate anions are entirely monomeric, and the other where they are derived from the type of linear silicate chain that is present in 1.4 nm tobermorite (and a number of other minerals); i.e. dreierkette-based models.

### 3.1. Models involving monomeric silicate anions

Bernal [164] considered that the greater part of the silica in the hydration products of a set cement is in the form of two hydrated calcium silicates, which were termed $C_2SH(II)$ and CSH(I). He speculated that both these phases included the monomeric silicate anion $[SiO_2(OH)_2]^{2-}$, and proposed the general formula given as Formula 1 in Table 2. Shpynova et al. [169] and Grudemo [176] also proposed models that involve monomeric silicate anions.

Both were derived from the structure of $Ca(OH)_2$ in an attempt to explain anomalous XRD peak intensities observed for $Ca(OH)_2$ in hardened cements. For example, in Shpynova's model $(OH)_4$ in the triple formula $Ca_3(OH)_6$ is replaced by $[SiO_4]$ giving — with some additional molecular water — $Ca_3[SiO_4](OH)_2{\cdot}2H_2O$ (Formula (3), Table 2). Whilst monomer is the only hydrated silicate species present during the induction period of hydrating $C_3S$, none of these monomer-based models are consistent with the experimentally observed distribution of silicate anions for the C-S-H that forms afterwards (see Section 3.3 in [189] for discussion).

### 3.2. Dreierkette-based models for C-S-H

The first dreierkette-based model for C-S-H was due to Bernal et al. [163]. They performed X-ray studies on hydrated $C_3S$ pastes and considered that the C-S-H phase formed was similar to C-S-H phases produced in dilute suspensions, which they called calcium silicate hydrates (I) and (II). Calcium silicate hydrate (I) had a layer structure, with the layers elongated in one direction that resulted in a fibrous structure,

Table 2
Summary of models for the nanostructure of C-S-H in hardened cements

| Year(s) | Author(s) | Ref | Based on structure of: | Silicate anion structure | Formulation or structure-composition equation | | Comments |
|---|---|---|---|---|---|---|---|
| 1952 | Bernal et al. | [163] | Tobermorite | Infinite | | | Infinite-chain models not consistent with experimentally observed distribution of silicate anions; i.e. $3n-1$ where $n$ is integer for individual structural units. |
| 1954 | Bernal | [164] | | Monomer | $Ca[SiO_2(OH)_2][Ca(OH)_2]_x[H_2O]_y$ | (1) | Monomeric models not consistent with experimentally observed distribution of silicate anions; i.e. $3n-1$ where $n$ is integer for individual structural units. |
| | | | | | $x$ would be 1 for $C_2SH(II)$ and between 0 and 0.5 for CSH(I) | | |
| 1956 | Taylor and Howison | [165] | Tobermorite | $3n-1$ | | | Ca/Si ratio raised above 0.83 by the removal of some 'bridging' tetrahedra and replacement by interlayer $Ca^{2+}$ ions |
| 1960,1962 | Kurczyk and Schwiete | [166,167] | Tobermorite | Infinite | $Ca[Ca_4Si_6O_{16}(OH)_2][Ca(OH)_2]_{5\rightarrow 7}\cdot mH_2O$ | (2) | $Ca^{2+}$ and $OH^-$ ions in an interlayer region, represented in their formula as $Ca(OH)_2$ groups, together with water molecules. Formula is consistent with Kantro et al.'s [1962] model in which layers of tobermorite are sandwiched between layers of calcium hydroxide. |
| 1967 | Shpynova et al. | [169] | $Ca(OH)_2$ | Monomer | $Ca_3[SiO_4](OH)_2\cdot 2H_2O$ | (3) | As Bernal (1954) above. |
| 1980–1987 | Stade and co-workers | [170–175] | Tobermorite | Dimer and polysilicate | $Ca_{4+y}(OH)_z\left[\left(H_{1+\frac{z}{2}}Si_2O_7\right)\right]_2\cdot mH_2O$ | (4) | Extension of Kurczyk and Schwiete's model by allowing silicate chains that are not infinite, and in particular dimeric. Limits on $y$ simply correspond to the compositions studied. |
| 1984 | Grudemo et al. | [176] | $Ca(OH)_2$ | Monomer | | | As Bernal (1954) above. |
| 1986 | Taylor | [177] | 1.4 nm tobermorite and jennite | ($3n$-1) | | | Structural elements based on 1.4 nm tobermorite and jennite (i.e. so-called T/J model). Fixed degree of protonation of the silicate chains. |
| 1987 | Glasser et al. | [178] | Tobermorite | Dimer | $Ca_xH_{6-2x}Si_2O_7\cdot zCa(OH)_2\cdot mH_2O$ | (5) | Derived from Stade and co-workers dimeric model, Formula (4) above (but z does not have the same definition as in Formula (4)). |
| 1992, 1993 | Richardson and Groves | [179,180] | Tobermorite, jennite, $Ca(OH)_2$ | ($3n$-1) | $Ca_XH_{(6n-2X)}\left(Si_{1-a}R_a^{[4]}\right)_{(3n-1)}O_{(9n-2)}\cdot I_{z(3n-1)}^{C+}\cdot zCa(OH)_2\cdot mH_2O$ | (6) | Includes both T/J and T/CH formulations; Formula (6) (with no substitution) is the polysilicate equivalent of Formula (5) (Glasser). |
| | | | | | $\left\{Ca_{2n}H_w(Si_{1-a}R_a^{[4]})_{(3n-1)}O_{9n-2}\right\}I_{z(3n-1)}^{C+}\cdot(OH)_{w+n(y-2)}\cdot Ca_{\frac{w}{2}}\cdot mH_2O$ | (7) | Variable degree of protonation of silicate chains. |
| | | | | | $Ca/Si=\frac{n(4+y)}{2(1-a)(3n-1)}$ $Ca/Si=\frac{n(4+y)+a(3n-1)}{2(1-a)(3n-1)}$ | (8)*and*(9) | Incorporation of substituent ions, most importantly substitution of $Si^{4+}$ by $Al^{3+}$. Possibility that T-, J- and CH-based structural elements co-exist. |
| 1993 | Taylor | [181] | Tobermorite and jennite | $3n-1$ | $Ca_4[(Si_{6-\Delta}\square_\Delta O_{18-2\Delta})H_{2p}Ca_{2-p}]_q\cdot(OH)_{8(1-q)}\cdot mH_2O$ | (10) | Formulation of 1986 model in response to Richardson and Groves' model, but extended to incorporate some of their modifications (variable protonation and substituents); as a consequence it is equivalent to Richardson and Groves' T/J formulation. |
| | | | | | $C/S=\frac{r}{\left(1-\frac{m}{3}\right)}$ $QRT=\frac{2}{\left(\frac{3}{m}-1\right)}$ | (11)*and*(12) | |
| 1996 | Cong and Kirkpatrick | [182,183] | Tobermorite | $3n-1$ | | | 'Defect tobermorite' model; Eqs. (11) and (12) are equivalent to equations in Richardson and Groves' 1992 model; see section 4.4.2 in Richardson (2004). |
| 1997–1999 | Grutzeck | [184,185] | Tobermorite, sorosilicate | Long-chain, dimer | $Ca_4(OH)_2[SiO_{3.5}]_2\cdot mH_2O$ | | Long-chain T-based phase with low Ca/Si and a dimeric sorosilicate-based phase with high Ca/Si. |
| 1998 | Nonat and Lecoq | [186] | Tobermorite | $3n-1$ | | | Two hypotheses: 1st equivalent to T units with $w/n=0$ and $y=2$ in Richardson and Groves' model (Formula (7) above); 2nd involves $Ca^{2+}$ and $OH^-$ ions in an interlayer region, in which respect it is similar to Kurczyk and Schwiete and Stade and co-workers. |
| 2004 | Chen, Thomas, Taylor, Jennings | [187] | Tobermorite and jennite | $3n-1$ | Chen et al. 's Table 5 presented formulae for mean chain lengths of 2, 3, 4, 5 and ∞ | | Formulae equivalent to T units with $w/n=0$ and $y=2$ in Richardson and Groves' model (Formula (7) above). |
| 2004 | Nonat | [188] | Tobermorite; jennite. | $3n-1$ | | | Update of 1998 model; mentions jennite-based structure. |

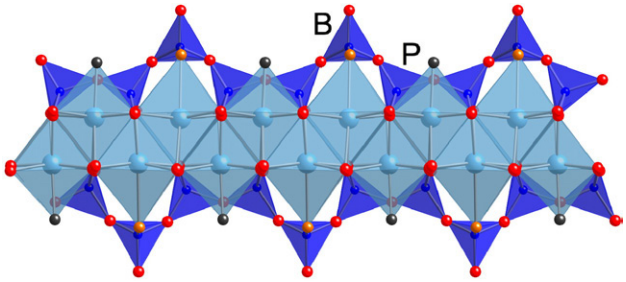


Fig. 1. Schematic diagram showing dreierkette chains present in tobermorite (which in theory are of infinite length). The chains have a kinked pattern where some silicate tetrahedra share O–O edges with the central Ca–O layer (called 'paired' tetrahedra (P)), and others that do not (called 'bridging' tetrahedra (B)).

and showed similarities to tobermorite, a rare crystalline calcium silicate hydrate that had been found in Northern Ireland ($Ca_4(Si_6O_{18}H_2)\cdot Ca\cdot 4H_2O$). Its structure — that was first described by Megaw and Kelsey [57] — is considered in more detail in Section 4. However, it is important to note here that it contains linear silicate chains of the 'dreierkette' form in which the silicate tetrahedra are co-ordinated to $Ca^{2+}$ ions by linking in such a way as to repeat a kinked pattern after every three tetrahedra. Two of the three tetrahedra share O–O edges with the central Ca–O part of the layer; these are linked together and are often referred to as 'paired' tetrahedra (P). The third tetrahedron, which shares an oxygen atom at the pyramidal apex of a Ca polyhedron, connects the two paired tetrahedra and so is termed 'bridging' (B). The dreierkette-type chain is illustrated in Fig. 1.

As long ago as 1956, Taylor and Howison [165] made the significant suggestion that the Ca/Si ratio could be raised above 0.83 — the value for Megaw and Kelsey's tobermorite — by the removal of some of the bridging tetrahedra and replacement by interlayer $Ca^{2+}$ ions; this mechanism for raising the Ca/Si ratio is a central feature of most dreierkette-based models. The various dreierkette-based models that have been proposed are listed in Table 2. Whilst the models might at first sight seem quite different from one another, they are in fact very similar. The similarities between some of them have already been discussed recently elsewhere [189], and those similarities will be only mentioned briefly here; the reader is therefore directed to reference [189] for the details. The models listed in Table 2 are considered in the following discussion in chronological order.

### 3.2.1. Kurczyk and Schwiete [166,167]

Kurczyk and Schwiete reported results of studies on both $C_3S$ and β-$C_2S$ pastes (water/cement = 0.5; 30 °C; hydrated 1, 2 and 3 months). The studies involved transmission electron microscopy (TEM) with selected area electron diffraction (SAED), thermal analysis, XRD and infrared spectroscopy. The Ca/Si ratios calculated from the XRD and thermal analysis were between 1.80 and 1.92. They suggested a hypothetical structure formula for the C-S-H that formed in both systems (that they referred to as a 'tobermorite-like phase') based on the same structural elements as determined by Megaw and Kelsey [57] to be present in tobermorite (i.e. single chains of dreierketten conformation). The tobermorite-like layers included ≡Si–OH groups and, since they were the same as in crystalline tobermorite, were presumably considered to be of infinite silicate chain length. The observed Ca/Si ratios were accounted for by the inclusion of $Ca^{2+}$ and $OH^-$ ions in an interlayer region, represented in their formula as $Ca(OH)_2$ groups, together with water molecules. Their formula, modified with the inclusion of the interlayer water, is given as Formula (2) in Table 2. This formula is consistent with Kantro et al.'s [168] model — which was proposed at around the same time —in which layers of tobermorite are sandwiched between layers of calcium hydroxide.

### 3.2.2. Stade and co-workers [170–175]

Like Kurczyk and Schwiete, Stade and Wieker [170] based their model on Megaw and Kelsey's proposal for the structure of tobermorite [57]. They envisaged that poorly crystalline and amorphous C-S-H phases are built up from $CaO_x$ polyhedra sandwiched between two silicate layers. Again, like Kurczyk

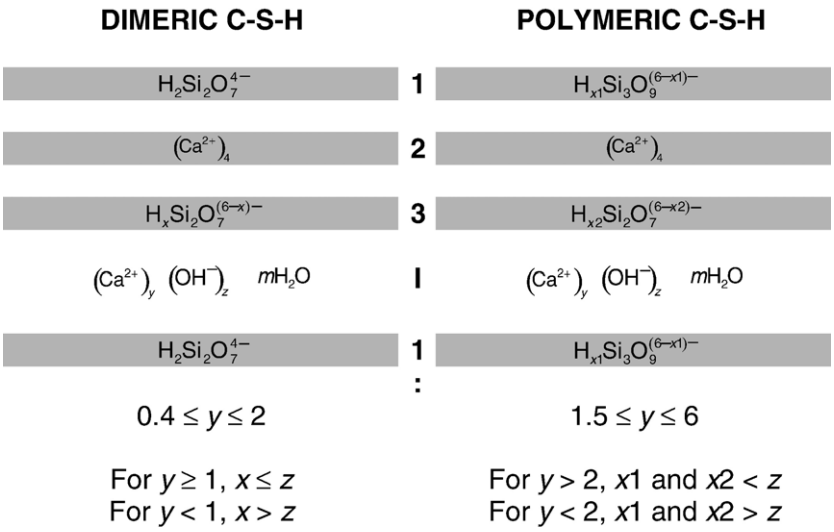


Fig. 2. Schematic representation of Stade and Wieker's model [170] illustrating the four-layer sequence (labelled as layers 1, 2, 3, and an intermediate layer, I).

Table 3
Calculated Ca/Si atom ratio and silicate chain length for the structural units envisaged in Taylor's model [177]. Taylor assumed that each unit had *n* silanol groups.

| Label | Ca/Si atom ratio | Chain length ($3n-1$) |
|---|---|---|
| J2 | 2.25 | 2 |
| J5 | 1.80 | 5 |
| J8 | 1.69 | 8 |
| J11 | 1.64 | 11 |
| J¥ | 1.50 | ∞ |
| T2 | 1.25 | 2 |
| T5 | 1.00 | 5 |
| T8 | 0.94 | 8 |
| T11 | 0.91 | 11 |
| T∞ | 0.83 | ∞ |

and Schwiete, these three-layer sequences are separated by an intermediate layer into which $H_2O$, $Ca^{2+}$, $OH^-$, and other ions may be incorporated to satisfy the observed composition. Their model extended Kurczyk and Schwiete's, however, in that it allows for their experimental observation that the silicate chains in their C-S-H were not infinite and in certain circumstances entirely dimeric. They expressed their model in two forms, one purely dimeric, and the other incorporating both dimer and polysilicate chains. The model is illustrated schematically in Fig. 2, which is based on figures in Stade [170]. The limits on *y* simply correspond to the compositions studied. The formula for purely dimeric C-S-H, as given by Stade and Wieker [170] is given as Formula (4) in Table 2. Garbev et al. [190] used Stade and Wieker's dimeric model in a recent paper and stated that the maximum possible Ca/Si ratio is 1.25. It must be emphasized that this is only the maximum because the dimeric silicate units in one of the layers in the model was fixed by Stade and Wieker as being totally protonated, see layer 1 in Fig. 2. Nevertheless, the formula given by Garbev et al. for Ca/Si ratio of 1.25 is useful in that it conveniently demonstrates the close similarity of Stade and Wieker's model with others: the formula is actually the same as that for Taylor's tobermorite-based dimer (see Section 3.2.3), or, in terms of Richardson and Groves' model [179] it corresponds to T-based units with $w/n=1$ and $y=1$.

### 3.2.3. Taylor [177]

Taylor's 1986 model, was a development of his earlier discussion, published 30 years earlier with Howison [165], that was mentioned above. The model envisages that C-S-H of high Ca/Si is composed of structural units derived from jennite and to a lesser extent 1.4 nm tobermorite [177]. The silicate chains present in jennite — which are in theory infinitely long — are similar to those in tobermorite, i.e. both are of the 'dreierkette' form. However, whilst in tobermorite the main layer consists of a central Ca−O part sandwiched between parallel silicate chains, in jennite half the oxygen atoms of the central component are part of −OH groups. The structure of jennite is discussed in Section 4.

The Ca/Si ratios of the structural units that result from the omission of bridging tetrahedra from the structures of 1.4 nm tobermorite and jennite vary linearly with the reciprocal of the silicate chain length; the values for the units derived assuming the level of protonation used by Taylor [177] are given in Table 3. To aid this discussion, the structural units derived from either jennite or 1.4-nm tobermorite are identified by the use of 'J' or 'T' as labels [179]. Hence, J2 and T2 correspond to dimeric structural units that result from omission of all bridging tetrahedra from jennite and tobermorite respectively, and J∞ and T∞ represent infinite chain lengths and so correspond to the crystalline phases themselves. The removal of numbers of bridging tetrahedra intermediate between none (infinite

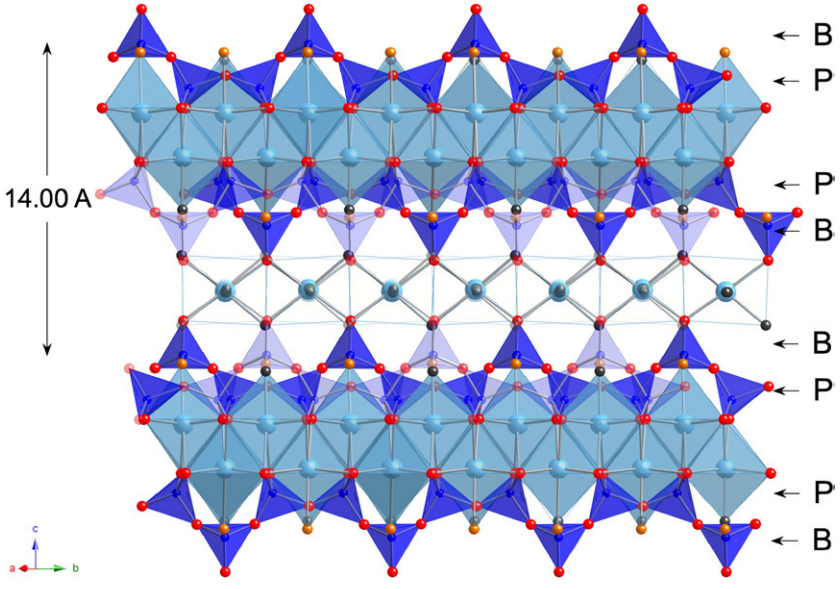


Fig. 3. Schematic diagram showing dreierkette chains present in 1.4 nm tobermorite projected along [210] (crystal structure data from [66] ). Note that the two sets of chains in the central part of the figure are not linked, but are offset from one another by *b*/2.

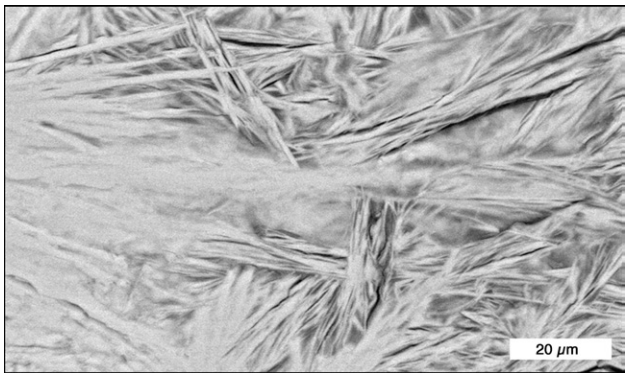


Fig. 4. Backscattered electron image of a region in a sample of 1.4 nm tobermorite from Crestmore, California. The image was obtained using a Philips XL-30 SEM operated at 20 kV.

length chains) and all (dimers) results in a sequence of finite silicate chains containing 2, 5, 8, …$3n-1$ tetrahedra (where $n=1, 2, 3, \ldots$), which is consistent with the silicate anion structure observed in hardened $C_3S$ and OPC pastes (see [155,189] and references therein). Taylor assumed that each bridging tetrahedron carries only one H atom, and that when one of these tetrahedra is missing only one of the broken ends of the chain is terminated by a H atom. Thus the net charge remains unchanged and the omission of a tetrahedron requires no change in the amount of interlayer Ca. He stated that, '*... there is no direct evidence for this assumption, but it is crystal-chemically reasonable and leads to a number of results that agree with experimental data.*' Taylor's model can thus be considered a special case of Richardson and Groves' T/J formulation (i.e. Formula (7) in Table 2), which allows greater flexibility in the degree of protonation of the silicate chains; the close relationship between the models is detailed in Section 4.4.1. of reference [189].

### 3.2.4. Glasser et al. [178]

Glasser et al. proposed a compositional model for dimeric C-S-H that seems to have been derived from Stade and co-workers' model. Whilst their thermodynamic treatment was strictly only applicable to precipitated gels with Ca/Si ratio between 1.0 and 1.4, they considered that the compositional model itself could be applied equally well to young C-S-H produced as a product of cement hydration. Glasser et al. referred to Stade and Wieker's formula (i.e. Formula (4) in Table 2) but stated that it was '*… difficult to write balanced equations based on this presentation for formation and dissolution equilibria of C-S-H.*' They represented their model by Formula (5) in Table 2 (note that $x$ and $z$ do not have the same definitions as those in Stade and Wieker's formula).

### 3.2.5. Richardson and Groves [179,180]

Richardson and Groves [179] proposed a generalized model that included formulations that could be interpreted from either the tobermorite-jennite (T/J) or tobermorite-'solid solution' $Ca(OH)_2$ (T/CH) viewpoints; indeed, it is possible that structural elements based on tobermorite, jennite (or jaffeite; see Section 4) and CH can all occur within the same system. The model includes maximum flexibility in the possible degree of protonation of the silicate chains, and it accounts for the substitution of $Al^{3+}$ for $Si^{4+}$ ions only at bridging sites [157,180], which is important for C-S-H present in cements containing fly ash, metakaolin or ground granulated blast-furnace

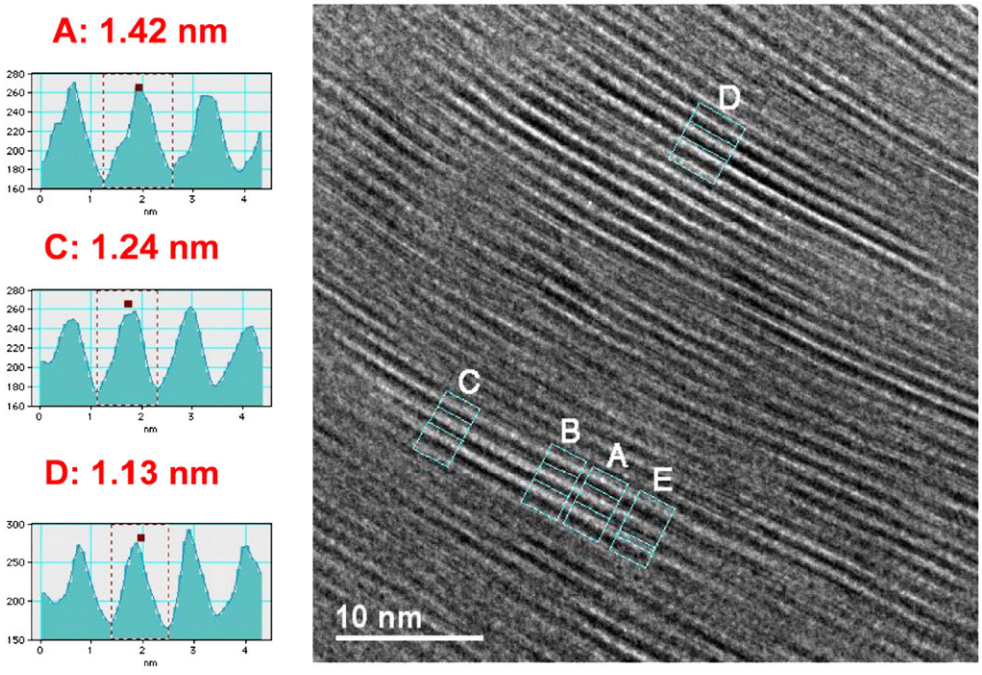


Fig. 5. High-resolution transmission electron micrograph of 1.4 nm tobermorite from Crestmore, California. The image was obtained using a Philips CM200 field emission TEM equipped with light element EDX detector.

slag, but which is not included in other models. The two formulations are given in Table 2 (Formulae (6) and (7)); Eqs. (8) and (9) are the composition–structure relationships where charge compensation of the substitution of $Al^{3+}$ for $Si^{4+}$ ions is entirely by alkali cations or $Ca^{2+}$ ions respectively. The close relationship between Richardson and Groves' formulations and the models due to Taylor [177], Cong and Kirkpatrick [182,183], Nonat and Lecoq [186] and Chen et al. [187] has been demonstrated in Richardson [189]. Glasser et al. 's [178] and Stade's [170] models are also closely related. The special case of Formula (6) for dimer ($n=1$) is the same as that given by Glasser et al. [178], Formula (5) (i.e. Formula (6) is essentially the polysilicate version of Glasser's compositional model for dimeric C-S-H) and Richardson and Groves' alternative formulation, Formula (7), reduces to Stade's dimeric model ($n=1$) if the number of silanol groups, $w$, is set equal to $(1+x/2)$ (like Taylor's model, Stade and Wieker's is less

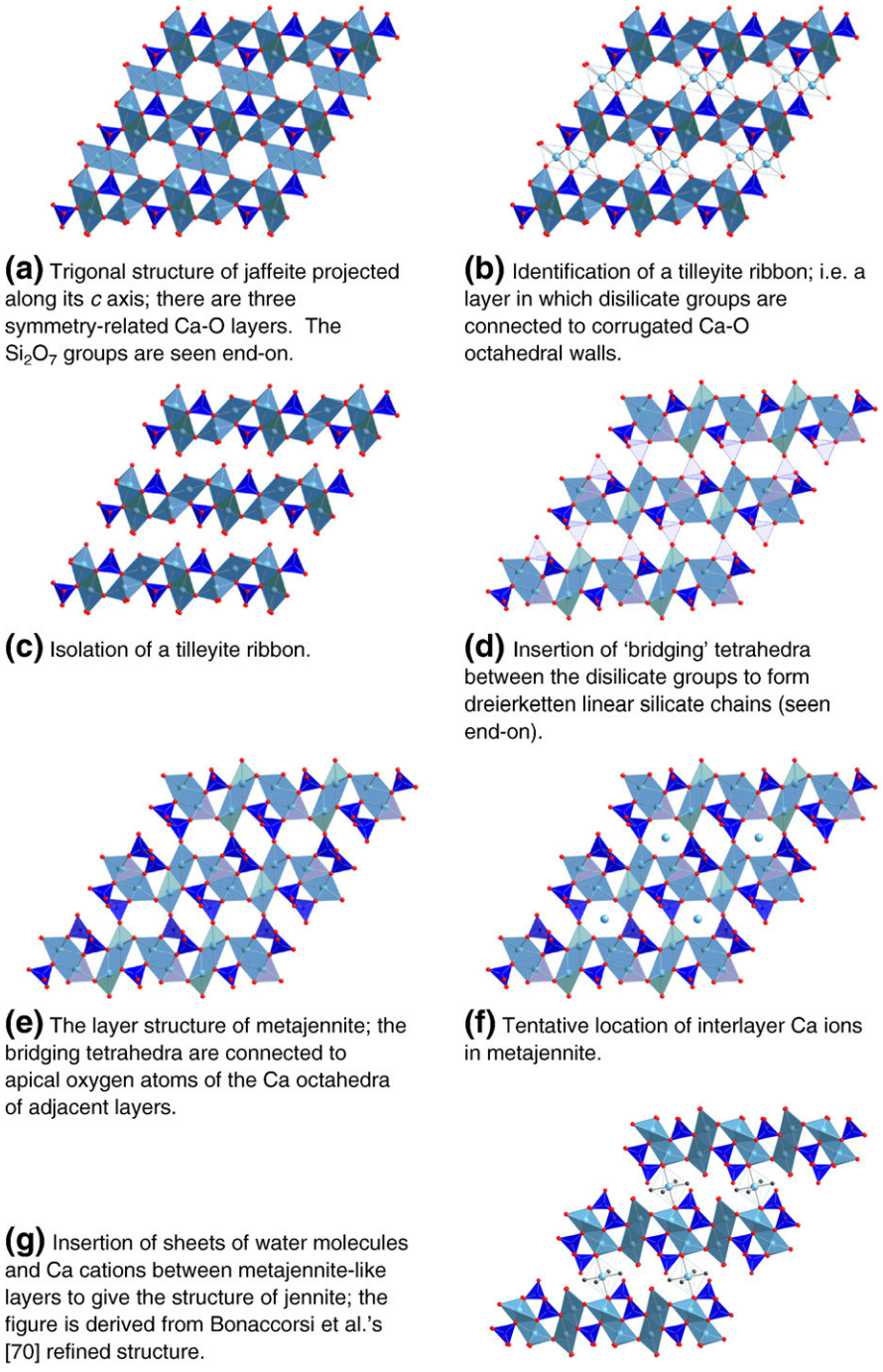


Fig. 6. Schematic diagrams illustrating the steps taken by Taylor in deriving his model structures for metajennite and jennite; Bonaccorsi et al. 's refined structure for jennite is shown in (g).

flexible than Richardson and Groves' in terms of the possible variation in the level of protonation of the silicate chains). Glasser's and Stade's models do not account for the $3n-1$ sequence of silicate chain lengths. Richardson and Groves' model is explained in detail with the extensive use of illustrative diagrams in reference [189].

### 3.2.6. Models of Cong and Kirkpatrick [182,183], Nonat and Lecoq [186] and Chen et al. [187]

As noted above, the similarities in the models of Cong and Kirkpatrick [182,183], Nonat and Lecoq [186] and Chen et al. [187] to the formulations of Richardson and Groves are discussed in detail in reference [189]; the reader is directed to that article.

## 4. Tobermorite (1.4 nm), jaffeite, metajennite and jennite

It is evident from Table 2 and the discussion in Section 3 that most models for the nanostructure of C-S-H in hardened Portland cement pastes involve elements of tobermorite-like structure. In a number of cases, these are intermixed with others of jennite-like structure (or jaffeite-like; see Section 4.2): the so-called tobermorite-jennite, or T/J, viewpoint [177,179]. As a consequence, perhaps two of the most significant papers for Cement Science that have been published since the 11th International Congress on the Chemistry of Cement are those by Bonaccorsi et al. that report refined crystal structures for 1.4 nm tobermorite [66] and jennite [70], which were determined with great skill using very small crystals.

### 4.1. Tobermorite (1.4 nm)

Bonaccorsi et al.'s determination of the structure of 1.4 nm tobermorite followed very extensive studies on other forms of tobermorite. The details of those structures have recently been reviewed and need no further summary here, other than to note that it includes a discussion of the reasons for so-called normal and anomalous behaviour and of the order–disorder (OD) character of phases in the tobermorite group [51]. The crystal structure of 1.4 nm tobermorite consists of the same complex layers that are present in 1.1 nm tobermorite: that is, it has a central Ca-O sheet that has silicate chains on both sides, which are kinked with a periodicity of three tetrahedra; these chains are called *dreierketten*, or wollastonite-like chains. The chemical composition of the complex layer is $[Ca_4Si_6O_{16}(OH)_2(H_2O)_4]^{2-}$. However, unlike 1.1 nm tobermorite, the silicate chains that belong to adjacent layers are not condensed into double chains, but are shifted by $b/2$ with respect to one another; the layers are also further apart, with the extra interlayer space occupied by $H_2O$ molecules and $Ca^{2+}$ ions. The structure is illustrated in Fig. 3.

As well Bonaccorsi et al. 's determination of the crystal structure of a sample of natural 1.4 nm tobermorite from Crestmore, California, another sample has also been characterized recently by analytical TEM and $^{29}$Si nuclear magnetic resonance spectroscopy (NMR) [63]. The single-pulse NMR spectrum was dominated by $Q^2$, indicating very long silicate chains; the authors were uncertain as to whether a small $Q^1$ peak was due to the 1.4 nm tobermorite or oyelite (i.e. 1.0 nm tobermorite). TEM-EDX gave a mean Ca/Si of 0.85 (SD = 0.03, $N=28$); the analyses ranged between 0.80 and 0.91. For comparison, another sample from Crestmore has been examined recently at the University of Leeds: the 1.4 nm tobermorite was intermixed with small amounts of oyelite and scawtite (on a host rock containing grossular, calcite, wollastonite, Mg silicate hydrate and scawtite). TEM-EDX gave a significantly lower mean Ca/Si of 0.80 (SD = 0.06, $N=19$) with a broader range of composition — between 0.70 and 0.96 — which suggests significant variation in protonation of the silicate chains (which $^{29}$Si NMR showed were essentially infinitely long (no $Q^1$)). Fig. 4 shows an illustrative backscattered electron micrograph of the tobermorite, which, together with bright field transmission electron micrographs (not shown) indicate that the tobermorite has lath and platy morphologies. The layer structure is illustrated in Fig. 5, which is a high-resolution transmission electron micrograph. This particular micrograph was taken as the crystal lost interlayer water under the electron beam, which resulted in a reduction in the layer spacing from 1.42 nm (e.g. A) to 1.24 nm (e.g. C) to 1.13 nm (e.g. D); this was followed by decomposition of the tobermorite structure. This sequence of dehydration steps is direct confirmation of the thermal analysis and XRD results reported by Yu and Kirkpatrick [60], which showed that upon heating water was lost in steps that corresponded to decreases in layer spacing from 1.4 to 1.2, 1.1 and 0.96 nm; the 1.2 nm stage was not noted by Bonaccorsi et al. [51]. It is of interest to note that the intermediate spacing of 1.24 nm is the same as the value typical of the basal spacing for semi-crystalline C-S-H that is often observed in alkali-activated hardened cements and in many synthetic C-S-H preparations, i.e. phases that give XRD patterns that match C-S-H (I), ICDD data set No. 34-0002.

### 4.2. Jaffeite, jennite and metajennite

Jennite is another crystalline calcium silicate hydrate that has dreierkette silicate chains, but it has a much higher Ca/Si ratio than tobermorite (formula $Ca_9Si_6O_{18}(OH)_6{\cdot}8H_2O$; Ca/Si ratio of 1.5). Taylor suggested a tentative crystal structure for

Table 4
The positions of the atoms in the asymmetric unit of Taylor's model structure for metajennite [75]

| Atom | Position | $x/a$ | $y/b$ | $z/c$ | Occ. |
|---|---|---|---|---|---|
| Ca1 | (4i) | 0.142 | 0 | 0.19 | 1 |
| Ca2 | (4i) | 0.788 | 0.5 | 0.165 | 1 |
| Ca3 | (2b) | 0 | 0.5 | 0 | 0.5 |
| Si1 | (8j) | 0.497 | 0.092 | 0.159 | 0.5 |
| Si2 | (4i) | 0.33 | 0.5 | 0.068 | 0.5 |
| O1 | (4i) | 0.206 | 0.5 | 0.11 | 1 |
| O2 | (4i) | 0.92 | 0 | 0.117 | 1 |
| O3 | (4i) | 0.652 | 0 | 0.188 | 1 |
| O4 | (4i) | 0.406 | 0 | 0.221 | 1 |
| O5 | (8j) | 0.425 | 0.125 | 0.081 | 0.5 |
| O6 | (4i) | 0.462 | 0.5 | 0.126 | 0.5 |
| O7 | (4i) | 0.734 | 0.5 | 0.023 | 1 |

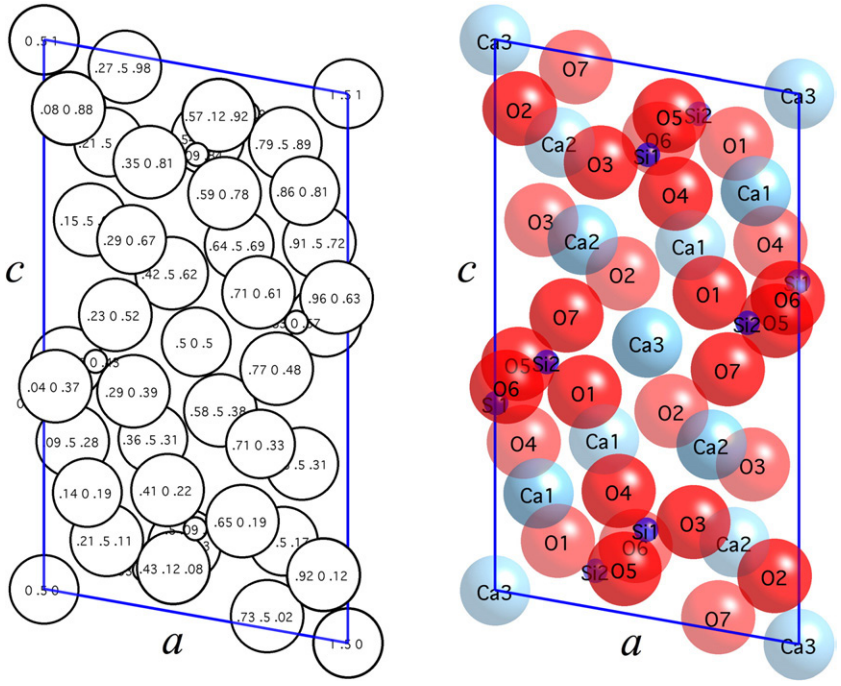


Fig. 7. The monoclinic structure of Taylor's metajennite projected along its *b* axis showing the positions of the atoms in the unit cell (data from [75] ). Co-ordinates (*x y z*) and atom labels are given in the left and right figures respectively.

jennite 40 years ago at the 5th International Symposium on the Chemistry of Cement [154], which included a central corrugated Ca−O sheet, but a full structure determination proved elusive because of the poor quality of available crystals. As noted above, perhaps one of the most significant papers for Cement Science that has been published since the last Congress is Bonaccorsi et al. 's refined crystal structure for jennite [70], which was determined using single crystal

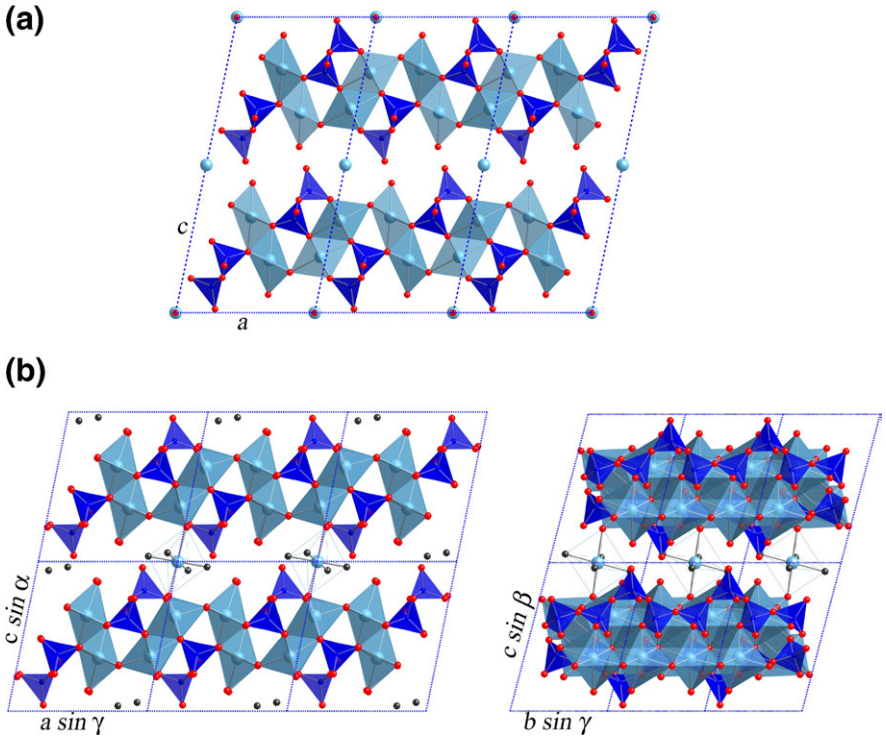


Fig. 8. (a) Taylor's model structure for jennite (average structure) viewed along [010]; the *dreierketten* chains are seen end-on (data from [75] ). (b) Bonaccorsi et al. 's refined structure for jennite (real structure) viewed along [010] (left) and [100] (data from [70] ).

X-ray diffraction data collected on a very thin crystal from Fuka, Japan. The paper includes a report of the development of a starting model for the structure, before describing the experimental work and the structural refinement. Hal Taylor was included posthumously as a co-author on the paper and the extent of his very significant contribution to the work was described by Bonaccorsi in an excellent presentation for the 1st H.F.W. Taylor Memorial Lecture, which was held during the 23rd Cement and Concrete Science conference, 8th–9th September 2003, University of Leeds. In fact, Taylor had progressed much further than his tentative structure of 1968: by the summer of 2000 he had determined trial substructures for both metajennite ($Ca_9Si_6O_{18}(OH)_6{\cdot}2H_2O$) — which is formed on heating jennite to 70–90 °C — and jennite itself. Taylor developed his model for the substructure of metajennite by assuming that it has a Ca − O structure similar to one of the three symmetry-related layers in jaffeite ($Ca_6[Si_2O_7](OH)_6$ [112] ), with its attached $Si_2O_7$ groups, and with the addition of bridging tetrahedra [75]. The steps taken by Taylor in deriving his model structure are represented schematically in Fig. 6.

The structure is monoclinic (space group I 1 2/*m* 1) with the lattice parameters given in Table 1 (i.e. those reported in [72] ). Taylor located 9 Ca, 6 Si and 26 O atoms in the subcell; the positions of the atoms in the asymmetric unit are given in Table 4, and are illustrated in Fig. 7, which is projected along its *b* axis. He noted that O3, O4, O5, and O6, and in 50% of cases, O1 and O7, are parts of silicate chains; that O2 is probably always OH, attached only to Ca; that where O1 is not in a silicate chain, it may be OH; and that where O7 is not in a silicate chain it may be water. The subcell contents and ionic constitution would therefore be $Ca_9Si_6O_{18}(OH)_6{\cdot}2H_2O$. Taylor also derived a model for the substructure of jennite, again using the parameters given in [72], essentially by the insertion

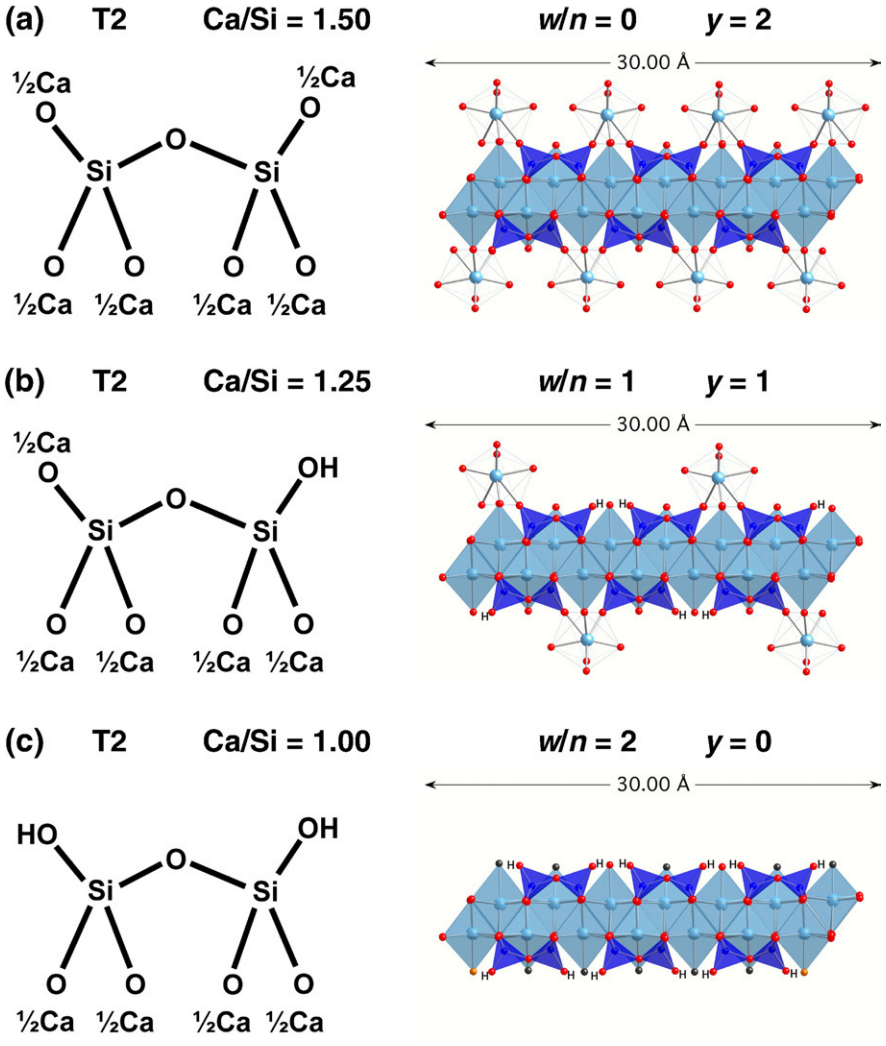


Fig. 9. Diagrams illustrating tobermorite-based dimer ($n = 1$) that has the minimum (a), intermediate (b), and maximum (c) degree of protonation of the silicate chains. The purpose of the highly schematic diagrams on the left-hand-side of the figure is to demonstrate chemical accounting; the values of the variables in Richardson and Groves' model [179] are indicated. The diagrams on the right-hand-side are more realistic structural representations that were derived from crystal-structure data for tobermorite [66] (the silicate chains are aligned along the plane of the page).

Table 5
Mean Ca/Si, Ca/(Al+Si) and Al/Si atom ratios for both Op and Ip C-S-H in the 4-year-old water-activated 70% WPC-30% fly ash blended cement paste obtained using TEM-EDX, and the Al/Si ratio determined by deconvolution of the single-pulse $^{29}$Si MAS NMR spectrum

| | | | Ca/Si | | Ca/(Al+Si) | | Al/Si | | |
|---|---|---|---|---|---|---|---|---|---|
| | | *N* | Mean | S.D. | Mean | S.D. | Mean | S.D. | NMR |
| Wpfa30 | Op | 20 | 1.40 | 0.18 | 1.19 | 0.10 | 0.18 | 0.07 | **0.18** |
| | Ip | 17 | 1.36 | 0.06 | 1.16 | 0.06 | 0.17 | 0.03 | |
| | All | 37 | 1.38 | 0.10 | **1.18** | 0.09 | **0.18** | 0.05 | |

(*N* = number of EDX analysis; S.D. = standard deviation).

of a layer of water molecules between metajennite-like layers, as illustrated in Fig. 6. Whilst the full solution and refinement of the structure of jennite was achieved with great experimental skill by Bonaccorsi — and is described in detail in [70] — it is apparent that the model structure derived by Taylor in 2000 was substantially correct, which is clearly apparent from Fig. 8.

## 5. Visualization of models for the nanostructure of C-S-H.

A consequence of the publication of the crystal structures of jaffeite [112], jennite [70], and 1.4 nm tobermorite [66] is that it is now much easier to build, display and manipulate the type of nanostructural units that are proposed in the various models for C-S-H. The result is that the similarities between the models are more readily apparent. An extensive set of illustrative figures is given in Richardson [189], which were derived from these structures, together with Taylor's trial structure for metajennite; three examples are given here, which are tobermorite-based (T-based) dimer (i.e. $n=1$) with different levels of protonation of the silicate chains (i.e. different values of $w/n$ in Richardson and Groves' model).

### *5.1. Example of similarity of models: T-based structural units with minimum degree of protonation ($w/n=0$)*

Fig. 9(a) shows T-based dimeric structural units that have the minimum degree of protonation; the Ca/Si ratio is 1.50 and in terms of Richardson and Groves' model $w/n=0$ and $y=2$. This unit is the same as:

(i) The formula for dimer in Chen et al. 's Table 5 [187], which was the result of their charge-balance arguments for the minimum Ca/Si ratios above which Ca-OH groups must be present;
(ii) Cong and Kirkpatrick's [182,183] model when 2C/S − NBO = 0;
(iii) Nonat and Lecoq's 'first hypothesis' [186,188].

### *5.2. Example of similarity of models: T-based structural units with intermediate degree of protonation ($w/n=1$)*

The structural units present in Taylor's 1986 model correspond to units in Richardson and Groves' model that have $w/n=1$ and $y=1$ for T-based units and $y=5$ for J-based; the T-based units are illustrated on Fig. 9(b), which have a Ca/Si ratio of 1.25. The similarity of the two models is easily demonstrated: substitution of $y=1$ or 5 and $n=1$, 2, 3, etc. into Formula (8) in Table 2 (and $a=0$, since there is no aluminium in Taylor's units) gives the Ca/Si ratios given in Table 3 (i.e. the values given in Taylor's paper). As noted above, the maximum Ca/Si ratio possible for dimer in Stade and co-workers' model also corresponds to $w/n=1$ and $y=1$.

### *5.3. Example of similarity of models: T-based structural units with maximum degree of protonation ($w/n=2$)*

Nonat updated his and Lecoq's 1998 model in 2004 [188]. The formula $Ca_2H_2Si_2O_7$ given by Nonat [188] on p1525 corresponds to T units with $w/n=2$ and $y=0$ in Formula (7) (illustrated in Fig. 9(c)). For Ca/Si ratios ≥ 1.5 Nonat incorporated what are essentially T/CH and T/J formulations. The paper includes the following on page 1526: '$Ca_3H_2Si_2O_7(OH)_2$ (Ca/Si = 1.5, one silicate bridging tetrahedron is be replaced by $Ca(OH)_2$ (tobermorite-like structure) or a non-bridging tetrahedron is replaced by $2OH^-$ (jennite-like part)'; on the T/J model this formula corresponds to $w/n=2$ and $y=2$; i.e. an equal mixture of T-based structure (represented by Fig. 9 (c), $y=0$) and J-based structure (represented by Fig. 29 in Richardson [189], $y=4$) that have maximum degree of

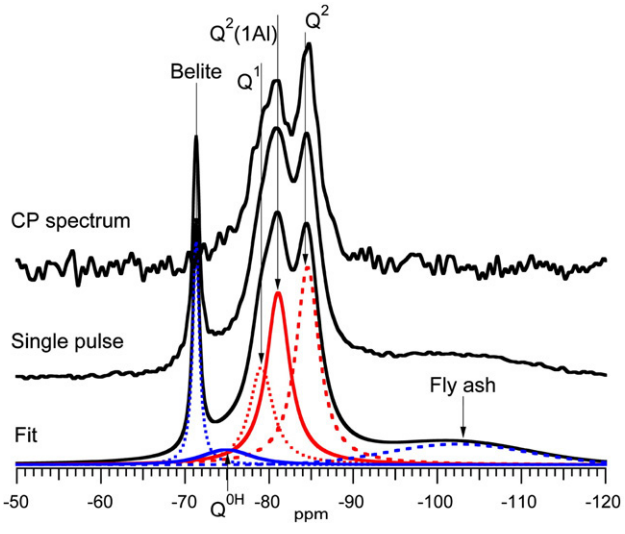


Fig. 10. Single-pulse $^{29}$Si (middle) and $^{1}$H-$^{29}$Si cross polarization (CP) (top) MAS NMR spectra for a water-activated 70% WPC-30% fly ash blend hydrated for 4 years at 25 °C. The spectra are scaled to their tallest peak. The result of the deconvolution of the single-pulse spectrum is shown at the bottom: the C-S-H peaks have chemical shifts of −79.1 ppm ($Q^1$), −81.1 ppm ($Q^2$(1Al)), and −84.6 ppm ($Q^2$(0Al)); there is a small $Q^{0H}$ peak at −75.0 ppm. The NMR spectra were acquired using a Varian InfinityPlus 300 spectrometer (magnetic field 7.05T; operating frequencies of 59.5 MHz for $^{29}$Si and 78.2 MHz for $^{27}$Al). The sample was freshly ground and packed into a 6 mm zirconia rotor sealed at either end with Teflon end plugs, and spun at 6 kHz in a Chemagnetics-style probe. The single-pulse spectrum was acquired over 27616 scans using a pulse recycle delay of 2 s, a pulse width of 4 μs and an acquisition time of 20 ms. The CP spectrum was acquired over 9440 scans with a contact time of 1 ms and a recycle delay of 2 s.

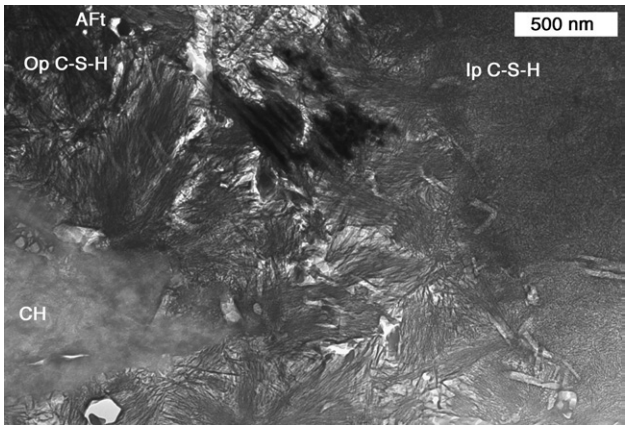


Fig. 11. TEM image from a water-activated 70% WPC-30% fly ash blend hydrated for 4 years at 25 °C. The outer product C-S-H has fine fibrillar morphology and the inner product has a fine homogeneous morphology. The region also contains CH crystals and AFt relicts.

protonation ($w/n=2$), and on the T/CH viewpoint it corresponds to $X=2$ and $z=1$ (i.e. substitution of $n=1$, $a=0$ (no aluminium), $X=2$ and $z=1$ into Formula (6) in Table 2 gives $Ca_2H_2Si_2O_7{\cdot}Ca(OH)_2$).

## 6. Example of the applicability of the models to C-S-H in hardened cements

A number of examples of the applicability of the models to C-S-H in hardened cements are given in Richardson [189], specifically regarding C-S-H present in hardened pastes of $C_3S$, $\beta$-$C_2S$, neat Portland cement and blends of Portland cement with blast-furnace slag, metakaolin, or silica fume. Additional examples have also recently been published for C-S-H in a 80% white Portland cement (WPC)-20% metakaolin blend hydrated at 25 °C [191], for neat Portland cement hydrated at 55 °C [192], a 70% WPC-30% fly ash blend hydrated at 85 °C [156], and in 20-year-old neat Portland cement and 10% WPC-90% blast-furnace slag pastes [193]. Another example is given here for C-S-H present in a 70% WPC-30% fly ash blend hydrated at 25 °C for 4 years.

Fig. 10 shows single-pulse $^{29}Si$ (middle) and $^{1}H$-$^{29}Si$ cross polarization (top) MAS NMR spectra for the paste; experimental details are given in the Figure caption. Deconvolution of the single-pulse spectrum gave a mean aluminosilicate chain length (MCL) of 11.3, the proportion of occupied bridging tetrahedra occupied by Al (rather than Si) was 57%, and the Al/Si ratio was 0.18.

Part of the sample was examined by TEM. The TEM micrograph in Fig. 11 shows a region with both fibrillar outer product (Op) C-S-H and fine and dense inner product (Ip) C-S-H. Large crystals of CH were also identified together with relicts of AFt; the hexagonal outline of an AFt relict near to the bottom left corner of the micrograph is particularly striking as it supports the view that the morphology of outer product C-S-H is not overly affected by the preparation procedure and high vacuum of the microscope (see discussion in [194] ). Areas of Ip and Op C-S-H were analysed by EDX (~200 nm in diameter). The data

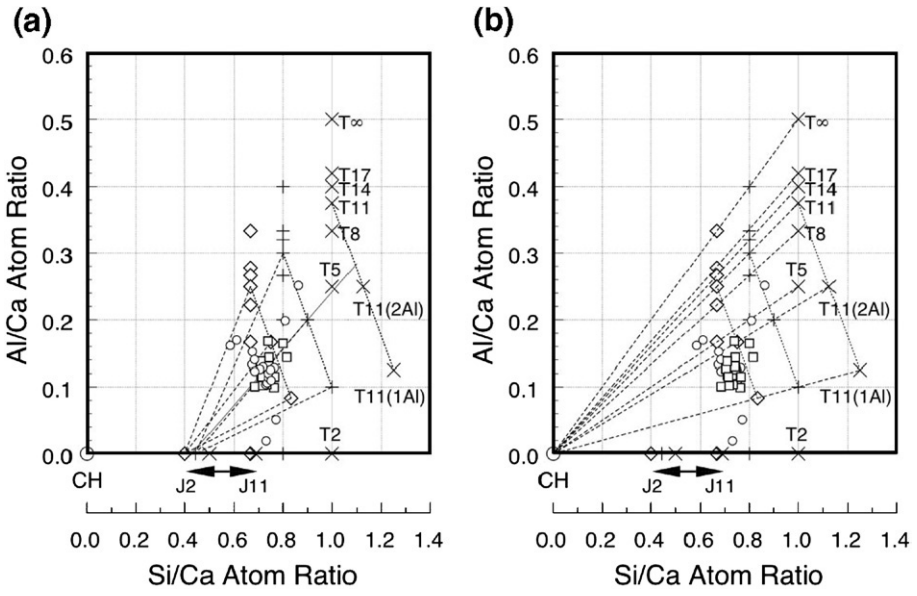


Fig. 12. (a) Al/Ca against Si/Ca atom ratio plot of TEM-EDX analyses of Ip (□) and Op (○) C-S-H present in the water-activated 70% WPC-30% fly ash blend hydrated for 4 years. The other symbols represent the compositions of tobermorite-(T) or jennite-/jaffeite-based (J) structural units with different levels of protonation of the silicate chains: the minimum level (◇; $w/n=0$), an intermediate level (+; $w/n=1$), and the maximum level (×; $w/n=2$). Points are included on the figures that represent tobermorite-based units with chain lengths of 2, 5, 8, 11, 14, 17 and ∞. Most of the units are saturated with Al (i.e. all the occupied bridging sites are occupied by Al rather than Si). The only exceptions are units with 11 tetrahedra, which in addition to those saturated with Al (i.e. Al/(Al+Si) = 3/11, which are labelled simply as T11), are also represented with one or two of the three bridging sites occupied by Al (i.e. Al/(Al+Si) = 1/11or 2/11): units with one or two Al ions are labelled as T11 (1Al) and T11(2Al) respectively. T11 units with the same degree of protonation but different content of Al are joined by dotted lines. The dashed tie lines join points for T11 structural units with points on the Si/Ca axis that represent jennite-based dimer (with different degrees of protonation). (b) As (a) except that the dashed tie lines now join points for structural units of the same length but different degrees of protonation with CH (at the origin).

are plotted as Al/Ca against Si/Ca scatter graphs in Fig. 12. The full line on Fig. 12(a) corresponds to the compositional relationship established in previous studies for C-S-H present in blast-furnace slag-Portland cement blends [195–200]: it is interesting to note that the compositions measured for this mature blend containing fly ash follows the same relationship. Mean values of Ca/Si, Ca/(Al+Si) and Al/Si ratios for C-S-H are given in Table 5. The Al/Si ratio measured in the TEM is in good agreement with that determined by deconvolution of the NMR spectrum.

The NMR and TEM-EDX data in Table 5 can be used to establish formulae for average structural units in the C-S-H in terms of the two alternative formulations for the nanostructure of C-S-H given by Richardson and Groves [179,180]; i.e. in terms of either the tobermorite-jennite (T/J) or tobermorite-calcium hydroxide (T/CH) structural viewpoints. The procedure to establish the structural formulae is straightforward: it simply involves calculation of the models' variables by inserting the experimentally determined mean values of Ca/Si and Al/Si ratios and aluminosilicate chain length into Formulae (6) and (7) given in Table 2. So, for example, an average structural unit with minimum degree of protonation of the aluminosilicate chains and assuming that the substitution of $Si^{4+}$ by $Al^{3+}$ is balanced entirely by $Ca^{2+}$ ions (i.e. using Eq. (9) to calculate $y$') can be represented by Eq. (13):

$$\{Ca_{8.2}(Si_{0.85}Al_{0.15})_{11.3}O_{34.9}\}\cdot(OH)_{0.25}\cdot Ca_{5.07}\cdot mH_2O \qquad (13)$$

The presence of hydroxyl groups outside the braces indicates that in terms of the T/J viewpoint, there must be some J-like structure. In terms of the T/CH viewpoint, the average structural unit is represented by (14):

$$Ca_{12.3}(Si_{0.85}Al_{0.15})_{11.3}O_{34.9}\cdot Ca_{0.85}\cdot 0.12Ca(OH)_2\cdot mH_2O \qquad (14)$$

It is evident from Formulae (13) and (14) that — if the aluminosilicate chains did indeed have a minimum degree of protonation — the C-S-H in this paste would consist mostly of T-based structure with little J- or CH-like structure necessary. Nevertheless, it is instructive to compare the distribution of the TEM-EDX analyses with the compositions of different units in Richardson and Groves' structural models: points that represent various structural units are included on Fig. 12; an explanation of the different symbols and tie lines on the figures is given in the caption. Each TEM-EDX data point corresponds to an analysis of C-S-H that had been checked by selected area electron diffraction to not be intermixed with a crystalline phase. The mean aluminosilicate chain length for the C-S-H was 11, with 57% of the occupied bridging sites occupied by Al; that is, an average structural unit would be a dreierkette chain with 11 tetrahedra with an $Al^{3+}$ ion at approximately two of the three bridging sites and $Si^{4+}$ at the other one. Consideration of the positions of the EDX data points with those of the structural units on Fig. 12 indicates that the C-S-H is likely to consist of structural units that are unprotonated, but it is not possible to decide whether there is a small amount of J- or CH-like structure. Nevertheless, it is clear that the relative positions of the TEM-EDX analyses and the theoretical T-based structural units are compatible with the data from the deconvolution of the NMR spectrum.

## 7. Size of particles of C-S-H in hardened $C_3S$ and neat Portland cement pastes

It was noted in the Introduction that a companion paper in this issue is concerned with the cohesion forces that act between individual layers or crystallites of C-S-H [5]; the purpose of this section is to lead into that paper by considering the size of individual particles of C-S-H. The example that is used to illustrate a small particle — which employs J-based (i.e. jaffeite- or jennite-based) type of structure for the C-S-H — also demonstrates possible reasons for the persistence of hydrated monomer in C-S-H and the fact that the extent of silicate polymerization is limited in systems with high Ca/(Si+Al) ratio.

In hardened cements there is a clear distinction between the morphology of C-S-H that forms in the originally water-filled space (outer product (Op) C-S-H) and the C-S-H that forms within the volume of the original particles (inner product (Ip) C-S-H). The Ip C-S-H generally has a very fine particulate morphology; the morphology of Op C-S-H is strongly dependent on chemical composition: at high Ca/(Si+Al) ratio it has a fibrillar morphology whereas with lower Ca/(Si+Al) it is foil- or sheet-like; many examples of TEM micrographs are given in Richardson [189,194] and references therein. Particles of C-S-H in water-activated $C_3S$, β-$C_2S$ and PC pastes appear to be very small. Ip C-S-H particles appear to be globular, around 3 to 8 nm in diameter. Op C-S-H particles appear to be long and thin, say 3 nm by some tens of nm; the fibrils of C-S-H consist of agglomerations of these thin particles. Particles of Ip C-S-H are smaller when formed at elevated temperature, which

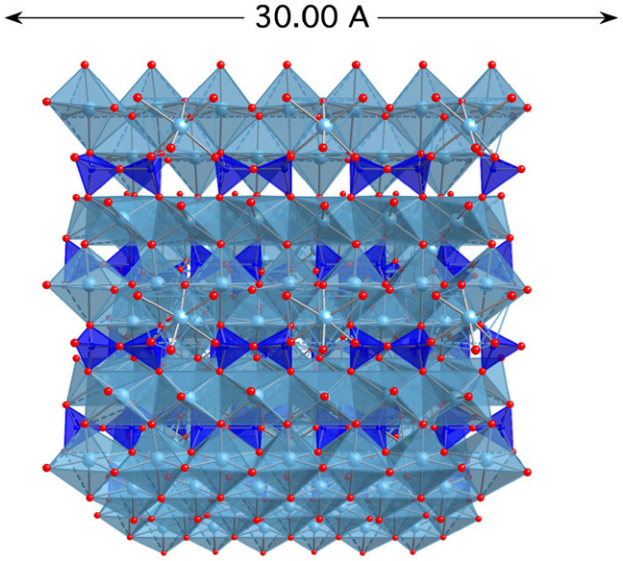


Fig. 13. Schematic diagram showing a view of an approximately 3-nm-sized particle, consisting entirely of J dimer with the minimum degree of protonation ($w/n=0$). The silicate chains are aligned across the page; a monomer is evident at the extreme right of the top row of silicate tetrahedra.

is illustrated in Figs. 7(b) and 9(b) of reference [189]. An approximately 3 nm-sized particle is shown in Fig. 13; the dimeric silicate chains are aligned along the plane of the page. The 3 nm size of the particle requires only two layers, which is more clearly apparent in Fig. 14(a), which shows the same particle as in Fig. 13 but rotated horizontally through 80°. In reality the adjacent layers are quite possibly not as close or aligned as shown; in this case they are as close as they can get to one another and well-ordered, betraying the model's origin (Ca-deficient jaffeite). Fig. 13 nicely illustrates that there is likely to be significant edge effects with such small particles of C-S-H: a monomer can be seen at the extreme right of the top row of silicate tetrahedra; this would seem to offer a reasonable explanation for the persistence of hydrated monomeric species. Certainly, it would explain why there is more hydrated monomer at elevated temperatures, where the particles seem to be smaller and apparently less in systems where the Op C-S-H has a foil-like morphology, which presumably has fewer chain-end edges than the particles in the fibrils present in water-activated $C_3S$ or PC pastes.

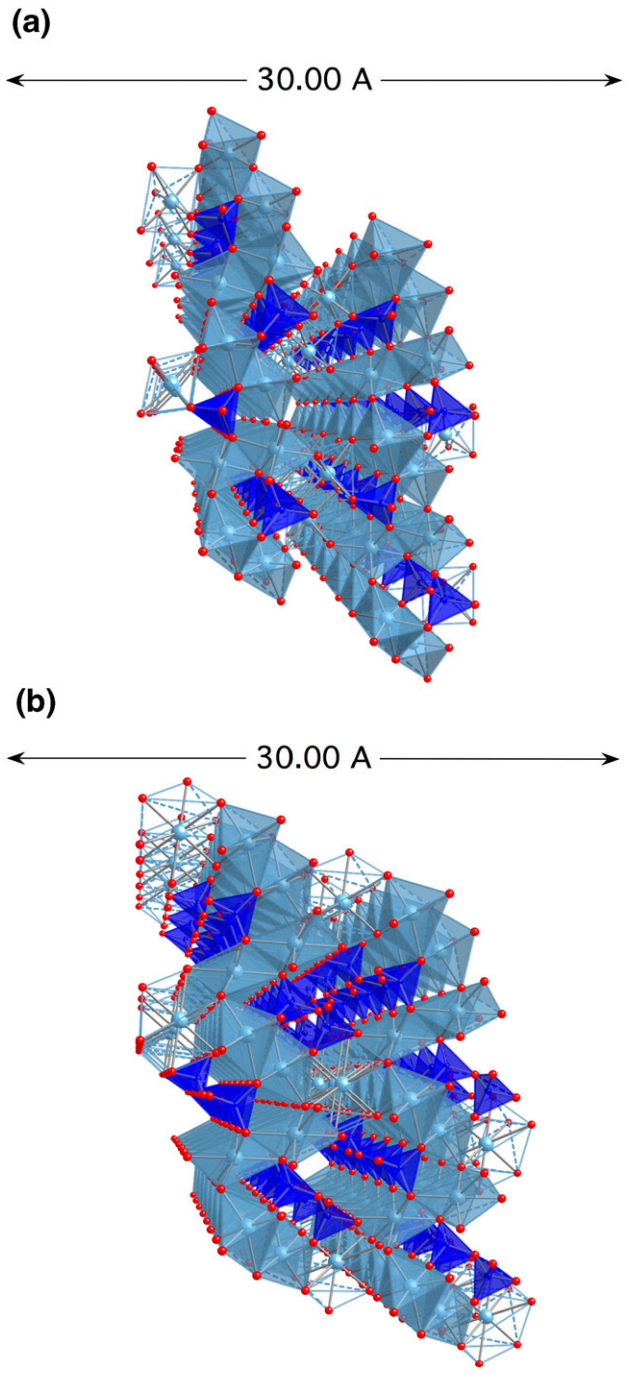


Fig. 14. (a) Schematic diagram showing the same J dimer-based particle as in Fig. 13, but rotated horizontally by 80°. (b) Essentially the same particle as in (a), but with silicate bridging tetrahedra now in place; i.e. the chains are fully polymerized.

Further consideration of this schematic representation of a C-S-H particle highlights an interesting point regarding the nature of polymerization in J-based structure. The same projection as in Fig. 14(a) is shown in Fig. 14(b) but this time with bridging tetrahedra replacing $Ca^{2+}$ ions, which have been displaced. This figure is derived from the model structure for metajennite (unrefined) produced by Taylor [75], who, as explained earlier, used jaffeite as a starting point; the relationship between the two structures is again clear from these two figures. It is equally clear that the displacement of $Ca^{2+}$ ions and the insertion of silicate tetrahedra would be easier at the surfaces of the particle than within its interior. This point is reinforced in reference [189], which has similar figures together with one derived from jennite itself (Fig. 38); in that case the main layers are much further apart. The point was made in that paper that it seems quite plausible that in an early-age particle that consists entirely of J dimer (with some associated monomer due to chain-end edge effects) the main layers would be closer together than in crystalline jennite, and that the subsequent insertion of bridging tetrahedra would therefore be much easier at the particle's surfaces (those that are not chain-end surfaces). It was noted that this is perhaps one reason why mean silicate chain lengths do not get above five in $C_3S$ pastes hydrated at ambient temperatures, but can get longer at higher temperatures where a smaller proportion of the silicate chains are in the interior of particles (because the particles are smaller).

## 8. Summary

This article is concerned with the calcium silicate hydrates, including crystalline minerals and the extremely variable and poorly ordered phase (C-S-H) that is essentially the 'glue' of the concrete part of the Built Environment. Up-to-date composition and crystal-structure information is tabulated for the most important crystalline calcium (alumino) silicate hydrates and related phases, which should be a useful reference source for others interested in these phases. A number of models for the nanostructure of C-S-H in hardened $C_3S$ and Portland cements — or in blends of Portland cement with supplementary cementing materials — have been published over the past 55 years. These models are summarized and compared and it is shown that many of them are in fact very similar to one another; i.e. there is much more of a consensus than might seem apparent at first sight. Illustrative examples are used to demonstrate the similarities. Most of the models involve elements of tobermorite-like structure. In a number of cases, these are intermixed with others of jennite-like structure. As a consequence, perhaps two

of the most significant papers for Cement Science that have been published since the 11th International Congress on the Chemistry of Cement are those by Bonaccorsi and co-workers that report refined crystal structures for 1.4 nm tobermorite and jennite. The value of these structures, together with those of jaffeite and metajennite, for visualizing the nanostructural elements present in the models is demonstrated. The importance of Hal Taylor's contribution to the solution of the structure of jennite is highlighted. The applicability of Richardson and Groves' model is demonstrated using experimental composition-structure observations on the nature of C-S-H present in a blended cement paste containing 30% fly ash, and attention is drawn to other examples published recently for C-S-H present in a range of systems. The stages in the dehydration of 1.4 nm tobermorite are illustrated using high-resolution transmission electron microscopy.

## Acknowledgements

Thanks are due to the Engineering and Physical Sciences Research Council for funding under Grant No. GR/S45874/01, to Dr. Andrew Brown for taking the HRTEM image and to Castle Cement, UK Nirex Ltd., and Lafarge Cements for the additional technical and financial support.

## References

[1] C.H. Desch, The mechanism of the setting process in plaster and cement, Trans. Faraday Soc. 14 (1–2) (1919) 1–7.
[2] H. Le Chatelier, Crystalloids against colloids in the theory of cements, Trans. Faraday Soc. 14 (1–2) (1919) 8–11.
[3] G.A. Rankin, The setting and hardening of Portland cement, Trans. Faraday Soc. 14 (1–2) (1919) 23–28.
[4] J.F. Young, Looking ahead from the past: The heritage pf cement chemistry, Cem. Concr. Res., this issue, doi:10.1016/j.cemconres.2007.09.011.
[5] R.J.-M. Pellenq, N. Lequeux, H. van Damme, Engineering the bonding scheme in C-S-H: the iono-covalent framework, Cem. Concr. Res., this issue, doi:10.1016/j.cemconres.2007.09.026.
[6] J.A. Gard, H.F.W. Taylor, The crystal structure of foshagite, Acta Crystallogr. 13 (1960) 785–793.
[7] A.S. Eakle, Foshagite, a new silicate from Crestmore, California, Am. Mineral. 10 (1925) 97–99.
[8] J.A. Gard, H.F.W. Taylor, Foshagite: composition, unit cell and dehydration, Am. Mineral. 43 (1958) 1–15.
[9] L. Black, K. Garbev, P. Stemmermann, K.R. Hallam, G.C. Allen, Characterisation of crystalline C-S-H phases by X-ray photoelectron spectroscopy, Cem. Concr. Res. 33 (2003) 899–911.
[10] C.L. Dickson, D.R.M. Brew, F.P. Glasser, Solubilities of $CaO–SiO_2–H_2O$ phases at 25, 55, 85 °C, Adv. Cem. Res 16 (2004) 35–43.
[11] Y.-S. Dai, J.E. Post, Crystal structure of hillebrandite: a natural analogue of calcium 5 silicate hydrate (CSH) phases in Portland cement, Am. Mineral., 80 (1995) 841–844.
[12] K.H. Mamedov, N.V. Belov, Crystal structure of hillebrandite, Dokl. Akad. Nauk SSSR, 123 (1958) 741–743 (in Russian).
[13] M.R. Hansen, H.J. Jakobsen, J. Skibsted, $^{29}Si$ chemical shift anisotropies in calcium silicates from high-field $^{29}Si$ NMR spectroscopy, Inorg. Chem. 42 (2003) 2368–2377.
[14] S.Y. Hong, F.P. Glasser, Phase relations in the $CaO–SiO_2–H_2O$ system to 200 °C at saturated steam pressure, Cem. Concr. Res. 34 (2004) 1529–1534.
[15] X. Hu, K. Yanagisawa, A. Onda, K. Kajiyoshi, Stability and phase relations of dicalcium silicate hydrates under hydrothermal conditions, J. Ceram. Soc. Jpn. 114 (2006) 174–179.
[16] Y. Okada, T. Masuda, H. Ishida, H. Nishido, Silicate anion structure and dehydration processes in okenite, J. Ceram. Soc. Jpn. 102 (1994) 919–924.
[17] K. Yanagisawa, X. Hu, A. Onda, K. Kajiyoshi, Hydration of β-dicalcium silicate at high temperatures under hydrothermal conditions, Cem. Concr. Res. 36 (2006) 810–816.
[18] A. Alberti, E. Galli, The structure of nekoite, $Ca_3Si_6O_{15}·7H_2O$, a new type of sheet silicate, Am. Mineral. 65 (1980) 1270–1276.
[19] J.A. Gard, H.F.W. Taylor, Okenite and nekoite (a new mineral), Mineral. Mag. 31 (1956) 5–20.
[20] R.A. Chalmers, A.W. Nicol, H.F.W. Taylor, The composition of nekoite, Mineral. Mag. 33 (1962) 70–71.
[21] R. Cerny, Powder pattern decomposition with the aid of preferred orientation — experimental test, Mat. Sci. Forum 321 (3) (2000) 22–27.
[22] S. Merlino, Okenite, $Ca_{10}Si_{18}O_{46}·18H_2O$: the first example of a chain and sheet silicate, Am. Mineral. 68 (1983) 614–622.
[23] J.A. Gard, H.F.W. Taylor, Okenite and nekoite (a new mineral), Mineral. Mag. 31 (1956) 5–20.
[24] Y. Takeuchi, Y. Kudoh, Hydrogen bonding and cation ordering in Magnet Cove pectolite, Z. Kristallog., Kristallg., Kristallp., Kristallch. 146 (1977) 281–292.
[25] M.J. Buerger, The determination of the crystal structure of pectolite, $Ca_2NaHSi_3O_9$, Z. Kristallogr. 108 (1956) 248–262.
[26] C.T. Prewitt, M.J. Buerger, Comparison of the crystal structures of wollastonite and pectolite, Mineral. Soc. Amer. Spec. Paper 1, 3rd General Meeting Int. Mineral. Ass., 1963, pp. 293–302.
[27] C.T. Prewitt, Refinement of the structure of pectolite, $Ca_2NaHSi_3O_9$, Z. Kristallogr. 125 (1967) 298–316.
[28] W.F. Müller, On stacking disorder and polytypism in pectolite and serandite. Z. Kristallogr., 144 (1976) 401–408.
[29] A. Sebald, L.H. Merwin, W.A. Dollase, F. Seifert, A multinuclear, high–resolution solid-state NMR study of sorensenite $(NaSnBe_2(Si_3O_9)·2H_2O)$ and comparison with wollastonite and pectolite, Phys. Chem. Miner. 17 (1990) 9–16.
[30] K. Baltakys, R. Siauciunas, The influence of γ-$Al_2O_3$ and $Na_2O$ on the formation of gyrolite in the stirring suspension, J. Mater. Sci. 41 (2006) 4799–4805.
[31] Y. Ohashi, Polysynthetically-twinned structures of enstatite and wollastonite, Phys. Chem. Miner. 10 (1984) 217–229.
[32] M.J. Buerger, C.T. Prewitt, The crystal structure of wollastonite and pectolite, Proc. Nat. Acad. Sci., 47 (1961) 1884–1888.
[33] C.T. Prewitt, M.J. Buerger, Comparison of the crystal structures of wollastonite and pectolite, Min. Soc. Am. Sp. Paper 1 (1963) 293–302.
[34] K. Lin, J. Chang, J. Lu, Synthesis of wollastonite nanowires via hydrothermal microemulsion methods, Mater. Lett. 60 (2006) 3007–3010.
[35] C. Hejny, T. Armbruster, Polytypism in xonotlite $Ca_6Si_6O_{17}(OH)_2$, Z. Kristallogr. 216 (2001) 396–408 polytype derived from structure in Kudoh and Takeuchi (1979).
[36] Y. Kudoh, Y. Takeuchi, Polytypism in xonotlite: (I) Structure of an A-1 polytype, Mineral. J. 9 (1979) 349–373.
[37] X. Li, J. Chang, A novel hydrothermal route to the synthesis of xonotlite nanofibres and investigation on their bioactivity, J. Mater. Sci. 41 (2006) 4944–4947.
[38] N. Meller, C. Hall, K. Kyritsis, G. Giriat, Synthesis of cement based on $CaO–Al_2O_3–SiO_2–H_2O$ (CASH) hydroceramics at 200 and 250 °C: Ex-situ and in-situ diffraction, Cem. Concr. Res. 37 (2007) 823–833.
[39] A. Hamilton, C. Hall, Physicochemical characterization of a hydrated calcium silicate board material, J. Building Phys. 29 (2005) 9–19.
[40] F. Meducin, B. Bresson, N. Lequeux, N. de Noirfontaine, H. Zanni, Calcium silicate hydrates investigated by solid-state high resolution $^1H$ and $^{29}Si$ nuclear magnetic resonance, Cem. Concr. Res. 37 (2007) 631–638.
[41] N. Meller, C. Hall, J. Phipps, A new phase diagram for the $CaO–Al_2O_3–SiO_2–H_2O$ hydroceramic system at 200 °C, Mater. Res. Bull. 40 (2005) 715–723.
[42] R. Siauciunas, K. Baltakys, Formation of gyrolite during hydrothermal synthesis in the mixtures of CaO and amorphous $SiO_2$ or quartz, Cem. Concr. Res. 34 (2004) 2029–2036.

[43] K. Luke, Phase studies of pozzolanic stabilized calcium silicate hydrates at 180 °C, Cem. Concr. Res. 34 (2004) 1725–1732.
[44] F.P. Glasser, S.Y. Hong, Thermal treatment of C-S-H gel at 1 bar $H_2O$ pressure up to 200 °C, Cem. Concr. Res. 33 (2003) 271–279.
[45] S. Shaw, S.M. Clark, C.M.B. Henderson, Hydrothermal formation of calcium silicate hydrates, Chem. Geol. 167 (2000) 129–140.
[46] S. Merlino, E. Bonaccorsi, T. Armbruster, The real structures of clinotobermorite and tobermorite 9 Å: OD character, polytypes, and structural relationships, Eur. J. Mineral. 12 (2000) 411–429.
[47] C. Henmi, I. Kusachi, Monoclinic tobermorite from Fuka, Bitchu-cho, Okayama Prefecture, Japan, J. Min. Petr. Econ. Geol. 84 (1989) 374–379 (In Japanese).
[48] C. Henmi, I. Kusachi, Clinotobermorite, $Ca_5Si_6(O,OH)_{18}\cdot 5H_2O$, a new mineral from Fuka, Okayama Prefecture, Japan, Mineral. Mag. 56 (1992) 353–358.
[49] C. Hoffmann, T. Armbruster, Clinotobermorite, $Ca_5[Si_3O_8(OH)]_2\cdot 4H_2O$–$Ca_5[Si_6O_{17}]\cdot 5H_2O$, a natural C-S-H(I) type cement mineral: determination of the substructure, Z. Kristallogr. 212 (1997) 864–873.
[50] S. Merlino, E. Bonaccorsi, T. Armbruster, Tobermorites: their real structure and order-disorder (OD) character, Am. Mineral. 84 (1999) 1613–1621.
[51] E. Bonaccorsi, S. Merlino, Modular microporous minerals: cancrinite-davyne group and C-S-H phases, Rev. Min. Geochem., 57 (2005) 241–290.
[52] L. Heller, H.F.W. Taylor, Crystallographic Data for the Calcium Silicates, H.M. Stationary Office, London, 1956, pp. 37–38, (10 Å tobermorite).
[53] I. Kusachi, C. Henmi, K. Henmi, An oyelite-bearing vein at Fuka, the town of Bitchu, Okayama Prefecture, Japan, J. Japan. Assoc. Min. Petr. Econ. Geol. 79 (1984) 267–275.
[54] J.D.C. McConnell, The hydrated calcium silicates riversideite, tobermorite, and plombierite, Mineral. Mag., 30 (1954) 293–305.
[55] H.F.W. Taylor, Crestmoreite and riversideite, Mineral. Mag. 30 (1953) 155–165.
[56] E. Bonaccorsi, S. Merlino, T. Armbruster, The real structure of tobermorite 11 Å: normal and anomalous forms, OD character and polytypic modifications, Eur. J. Mineral., 13 (2001) 577–590.
[57] H.D. Megaw, C.H. Kelsey, Crystal structure of tobermorite, Nature, 177 (1956) 390–391.
[58] T. Mitsuda, H.F.W. Taylor, Normal and anomalous tobermorites, Mineral. Mag., 42 (1978) 229–235.
[59] S.A. Hamid, The crystal structure of 11 Å natural tobermorite $Ca_{2.25}[Si_3O_{7.5}(OH)_{1.5}]\cdot 1H_2O$, Z. Kristallogr. 154 (1981) 189–198.
[60] P. Yu, R.J. Kirkpatrick, Thermal dehydration of tobermorite and jennite, Concr. Sci. Eng., 1 (1999) 185–191.
[61] L. Black, A. Stumm, K. Garbev, P. Stemmermann, K.R. Hallam, G.C. Allen, X-ray photoelectron spectroscopy of aluminium-substituted tobermorite, Cem. Concr. Res. 35 (2005) 51–55.
[62] N.J. Coleman, Synthesis, structure and ion exchange properties of 11 Å tobermorites from newsprint recycling residue, Mater. Res. Bull. 40 (2005) 2000–2013.
[63] T. Maeshima, H. Noma, M. Sakiyama, T. Mitsuda, Natural 1.1 and 1.4 nm tobermorites from Fuka, Okayama, Japan: Chemical analysis, cell dimensions, 29Si NMR and thermal behaviour, Cem. Concr. Res. 33 (2003) 1515–1523.
[64] F. Sato, G. Mi, M. Hanada, Mechanochemical synthesis of hydrated calcium silicates by room temperature grinding, Solid State Ion. 101–103 (1997) 37–43.
[65] R. Siauciunas, A. Baltusnikas, Influence of $SiO_2$ modification on hydrogarnets formation during hydrothermal synthesis, Cem. Concr. Res. 33 (2003) 1789–1793.
[66] E. Bonaccorsi, S. Merlino, A.R. Kampf, The crystal structure of tobermorite 14 Å (plombierite), a C-S-H phase, J. Am. Ceram. Soc. 88 (2005) 505–512.
[67] J.D.C. McConnell, The hydrated calcium silicates riversideite, tobermorite, and plombierite, Mineral. Mag. 30 (1954) 293–305.
[68] J.D.C. McConnell, The hydration of larnite (b-$Ca_2SiO_4$) and bredigite ($a_1$-$Ca_2SiO_4$) and the properties of the resulting gelatinous mineral plombierite, Mineral. Mag., 30 (1955) 672–680.
[69] S. Gross, The mineralogy of the Hatrurim Formation, Israel. Geol. Sur. Israel Bull., 70 (1977) 47.
[70] E. Bonaccorsi, S. Merlino, H.F.W. Taylor, The crystal structure of jennite, $Ca_9Si_6O_{18}(OH)_6\cdot 8H_2O$, Cem. Concr. Res. 34 (2004) 1481–1488.
[71] A.B. Carpenter, R.A. Chalmers, J.A. Gard, K. Speakman, H.F.W. Taylor, Jennite, a new mineral, Am. Mineral. 51 (1966) 56–74.
[72] J.A. Gard, H.F.W. Taylor, G. Cliff, G.W. Lorimer, A re-examination of jennite, Am. Mineral. 62 (1977) 365–368.
[73] I. Kusachi, C. Henmi, K. Henmi, Afwillite and jennite from Fuka, Okayama Province, Japan, Mineral. J. (Japan) 14 (1989) 279–292.
[74] E. Bonaccorsi, S. Merlino, H.F.W. Taylor, Crystal structures of jennite and tobermorites: New data for understanding the nanostructure of Portland cement. Paper presented at Congress of the Italian Association of Crystallography, 2002.
[75] H.F.W. Taylor, Personal communication, 2000.
[76] R.H. Mitchell, P.C. Burns, The structure of fedorite: a reappraisal, Canadian Mineral. 39 (2001) 769–777.
[77] G.V. Sokolova, A.A. Kashayev, V.A. Drits, V.V. Ilyukhin, The crystal structure of fedorite, Krisallografiya 28 (1983) 170–172.
[78] S. Merlino, Gyrolite: its crystal structure and crystal chemistry, Mineral. Mag., 52 (1988) 377–387.
[79] A.L. Mackay, H.F.W. Taylor, Gyrolite, Mineral. Mag. 30 (1953) 80–91.
[80] J.W. Meyer, K.L. Jaunarajs, Synthesis and chemistry of gyrolite and reyerite, Am. Mineral. 46 (1961) 913–933.
[81] J.A. Gard, T. Mitsuda, H.F.W. Taylor, Some observations on Assarsson's Z-phase and its structural relations to gyrolite, truscottite, and reyerite, Mineral. Mag. 40 (1975) 325–333.
[82] S. Shaw, C.M.B. Henderson, S.M. Clark, In situ synchrotron study of the kinetics, thermodynamics, and reaction mechanisms of the hydrothermal characterization of gyrolite, Am. Mineral. 87 (2002) 533–541.
[83] A. Stumm, K. Garbev, G. Beuchle, L. Black, P. Stemmermann, R. Nuesch, Incorporation of zinc into calcium silicate hydrates, Part I: formation of C-S-H(I) with C/S=2/3 and its isochemical counterpart gyrolite, Cem. Concr. Res. 35 (2005) 1665–1675.
[84] S. Merlino, The structure of reyerite, $(Na,K)_2Ca_{14}Si_{22}Al_2O_{58}(OH)_8\cdot 6H_2O$, Mineral. Mag. 52 (1988) 247–256.
[85] R.A. Chalmers, V.C. Farmer, R.I. Harker, S. Kelly, H.F.W. Taylor, Reyerite, Mineral. Mag. 33 (1964) 821–840.
[86] S.C. Clement, P.H. Ribbe, New locality, formula, and proposed structure for reyerite, Am. Mineral. 58 (1973) 517–522.
[87] A.L. Mackay, H.F.W. Taylor, Truscottite, Mineral. Mag. 30 (1954) 450–457.
[88] E.E. Lachowski, L.W. Murray, H.F.W. Taylor, Truscottite: composition and ionic substitutions, Mineral. Mag. 43 (1979) 333–336.
[89] T.P. Kuznetsova, N.N. Nevskii, V.V. Ilyukhin, N.V. Belov, Refinement of the crystal structure of calcium chondrodite, $Ca_5[SiO_4]_2(OH)_2$=$Ca(OH)_2\cdot Ca_2SiO_4$, Soviet Physics Crystallography, 25 (1980) 91–92 (translation of Kristallografiya, 25 (1980) 159–160).
[90] E.R. Buckle, H.F.W. Taylor, A calcium analogue of chondrodite, Am. Min. 43 (1958) 818–823.
[91] R.M. Ganiev, Yu.A. Kharitonov, V.V. Ilyukhin, N.V. Belov, Crystal structure of calcium chondrodite, $Ca_5[SiO_4]_2(OH)_2$=$Ca(OH)_2\cdot Ca_2SiO_4$, Soviet Physics – Doklady, 14 (1970) 946–948 (translation of Dokl. Acad. Nauk SSSR, 188 (1969) 1281).
[92] H.-M. Hamm, G. Hentschel, Reinhardbraunsite, $Ca_5(SiO_4)_2(OH,F)_2$, a new mineral equivalent of synthetic 'calcio-chondrodite', Neues Jahrb. Mineral., Monatsh. (1983) 119–129.
[93] A. Kirfel, H.-M. Hamm, G. Will, The crystal structure of reinhardbraunsite, $Ca_5(SiO_4)_2(OH,F)_2$; a new mineral of the calcio-chondrodite type, Tschermaks Mineral. Petrogr. Mitt. 31 (1983) 137–150.
[94] H.F.W. Taylor, The crystal structure of Kilchoanite, $Ca_6(SiO_4)(Si_3O_{10})$, with some comments on related phases, Mineral. Mag. 38 (1971) 26–31.
[95] K.M.A. Malik, J.W. Jeffrey, A re-investigation of the structure of afwillite, Acta Crystallogr. 32 (1976) 475–480.
[96] J. Parry, F.E. Wright, Afwillite, a new hydrous calcium silicate from Dutoitspan Mine, Kimberley, South Africa, Mineral. Mag. 20 (1925) 277–285.

[97] H.D. Megaw, The structure of afwillite, $Ca_3(SiO_3OH)_2(H_2O)_2$, Acta Crystallogr. 5 (1952) 477–491.
[98] G. Switzer, E.H. Bailey, Afwillite from Crestmore, California, Am. Mineral. 38 (1953) 629–633.
[99] L. Heller, H.F.W. Taylor, Crystallographic Data for the Calcium Silicates, H.M. Stationary Office, London, 1956, pp. 50–53.
[100] I. Kusachi, C. Henmi, K. Henmi, Afwillite and jennite from Fuka, Okayama Prefecture, Japan, Mineral. J. (Japan) 14 (1989) 279–292.
[101] R.E. Marsh, A revised structure for a-dicalcium silicate hydrate, Acta Crystallogr. C50 (1994) 996–997.
[102] H. Heller, The structure of dicalcium silicate a-hydrate, Acta Crystallogr. 5 (1952) 724–728.
[103] T. Yano, K. Urabe, H. Ikawa, T. Teraushi, N. Ishizawa, S. Udagawa, Structure of a-dicalcium silicate hydrate, Acta Crystallogr. C49 (1993) 1555–1559.
[104] B. Bresson, F. Meducin, H. Zanni, C. Noik, Hydration of tricalcium silicate ($C_3S$) at high temperature and high pressure, J. Mater. Sci. 37 (2002) 5355–5365.
[105] S. Saburi, A. Kawahara, C. Henmi, I. Kusachi, K. Kihara, The refinement of the crystal structure of cuspidine, Mineral. J. (Japan), 8 (1977) 286–298.
[106] C.E. Tilley, Cuspidine from dolomite contact skarns, Broadford, Skye. Mineral. Mag. 28 (1947) 90–95.
[107] R.F. Smirnova, I.M. Rumanova, N.V. Belov, The crystal structure of cuspidine, Zap. Vses. Mineral. Obsestva 84 (1955) 159–169.
[108] A. Van Valkenberg, G.F. Rynders, Synthetic cuspidine, Am. Mineral. 43 (1958) 1195–1202.
[109] A.N. Safronov, N.N. Nevsky, V.V. Ilyukhin, N.V. Belov, The refinement of the crystal structure of the cement phase gamma-$C_6S_3H$, Dokl. Akad. Nauk SSSR 256 (1981) 1387–1389.
[110] S.O. Agrell, Polythermal metamorphism of limestones at Kilchoan, Ardnamurchan. Mineral. Mag. 34 (1965) 1–15.
[111] R.M. Ganiev, V.V. Ilyukhin, N.V. Belov, Crystal structure of cement phase Y = $Ca_6(Si_2O_7)(SiO_4)(OH)_2$, Dokl. Akad. Nauk SSSR 190 (1970) 831–834.
[112] N.A. Yamnova, Kh. Sarp, Yu. K. Egorov-Tismenko, D.Yu. Pushcharovskii, Crystal structure of jaffeite, Crystallogr. Rep 38 (1993) 464–466 (c/c of Kristallografiia).
[113] H. Sarp, D.R. Peacor, Jaffeite, a new hydrated calcium silicate from the Kombat mine, Namibia. Am. Mineral. 74 (1989) 1203–1206.
[114] H.F.W. Taylor, The crystal structure of killalaite, Mineral. Mag. 41 (1977) 363–369.
[115] R. Nawaz, Killalaite, a new mineral from Co. Sligo, Ireland, Mineral. Mag. 39 (1974) 544–548.
[116] Y.-S. Dai, G.E. Harlow, A.R. McGhie, Poldervaartite, $Ca(Ca_{0.5}Mn_{0.5})(SiO_3(OH))(OH)$, a new acid nesosilicate from the Kalahari manganese field, South Africa: crystal structure and description, Am. Mineral. 78 (1993) 1082–1087.
[117] C. Wan, S. Ghose, G.V. Gibbs, Rosenhahnite, $Ca_3Si_3O_8(OH)_2$:crystal structure and the stereochemical configuration of the hydroxylated trisilicate group, $[Si_3O_8(OH)_2$, Am. Mineral. 62 (1977) 503–512.
[118] A. Pabst, E.B. Gross, J.T. Alfors, 'Rosenhahnite, a new hydrous calcium silicate from Mendocino County, California', Am. Mineral. 52 (1967) 336–351.
[119] J.W. Jeffery, P.F. Lindley, Remarkable new structure, Nature 241 (1973) 42–43.
[120] J.V. Oglesby, J.F. Stebbins, $^{29}$Si CPMAS NMR investigations of silano-group minerals and hydrous aluminosilicate glasses, Am. Mineral. 85 (2000) 722–731.
[121] Z. Ma, N. Shi, G. Mou, L. Liau, Crystal structure refinement of suolunite and its significance to the cement techniques, Chin. Sci. Bull. 44 (1999) 2125–2130.
[122] Y. Huang, Suolunite — a new mineral, The Geological Review 23 (1965) 7 (in Chinese).
[123] J. Tseng, C. Hsueh, C. Peng, The crystal structure of suolunite, Kexue Tongbao 17 (1966) 45–48.
[124] Anon, The X-ray Laboratory of Hubei Geological Institute), the crystal structure of suolunite, Sci. Geol. Sin. 2 (1974) 117–132 (in Chinese).
[125] G. Stanger, C. Neal, A new occurrence of suolunite, from Oman, Mineral. Mag. 48 (346) (1984) 143–146.
[126] S.J. Louisnathan, J.V. Smith, Crystal structure of tilleyite: refinement and coordination, Z. Kristallogr. 132 (1970) 288–306.
[127] J.D. Grice, The structure of spurrite, tilleyite and scawtite, and relationships to other silicate-carbonate minerals, Canadian Mineral. 43 (2005) 1489–1500.
[128] S. Medvescek, R. Gabrovsek, V. Kaucic, A. Meden, Hydration products in water suspension of Portland cement containing carbonates of various solubility, Acta Chim. Slov. 53 (2006) 172–179.
[129] S.E. Dann, P.J. Mead, M.T. Weller, Lowenstein's rule extended to an aluminium rich framework. The structure of bicchulite, $Ca_8(Al_2SiO_6)_4(OH)_8$, by MASNMR and neutron diffraction, Inorg. Chem. 35 (1996) 1427–1428.
[130] K. Sahl, N.D. Chaterjee, Crystal structure of bicchulite $Ca_2(Al_2Si\ O_6)(OH)_2$, Z. Kristallogr. 146 (1977) 35–41.
[131] K. Sahl, Refinement of the crystal structure of bicchulite $Ca_2(Al_2Si\ O_6)(OH)_2$, Z. Kristallogr. 152 (1980) 13–21.
[132] B. Winkler, V. Milman, C.J. Pickard, Quantum mechanical study of Al/Si disorder in leucite and bicchulite, Mineral. Mag. 68 (2004) 819–824.
[133] R.K. Rastsvetaeva, N.B. Bolotina, A.E. Zadov, N.V. Chukanov, Crystal structure of fukalite dimorph $Ca_4(Si_2O_6)(CO_3)(OH)_2$ from the Gumeshevsk deposit, the Urals, Dokl. Earth Sci. 405 (2005) 1347–1351.
[134] C. Henmi, I. Kusachi, A. Kawahara, K. Henmi, Fukalite, a new calcium carbonate silicate hydrate mineral, Mineral. J. 8 (1977) 374–381 (Japan).
[135] O. Ferro, E. Galli, G. Papp, S. Quartieri, S. Szakáll, G. Vezzalini, A new occurrence of katoite and re-examination of the hydrogrossular group, Eur. J. Mineral. 15 (2003) 419–426.
[136] G.A. Lager, W.G. Marshall, Z. Liu, R.T. Downs, Re-examination of the hydrogarnet structure at high pressure using neutron powder diffraction and infrared spectroscopy, Am. Mineral. 90 (2005) 639–644.
[137] G. Le Saout, E. Lecolier, A. Rivereau, H. Zanni, Chemical structure of cement aged at normal and elevated temperatures and pressures Part I. Class G oilwell cement, Cem. Concr. Res. 36 (2006) 71–78.
[138] G. Le Saout, E. Lecolier, A. Rivereau, H. Zanni, Chemical structure of cement aged at normal and elevated temperatures and pressures, Part II: Low permeability class G oilwell cement, Cem. Concr. Res. 36 (2006) 428–433.
[139] J.M.R. Mercury, P. Pena, A.H. De Aza, X. Turrillas, I. Sobrados, J. Sanz, Solid-state Al-27 and Si-29 NMR investigations on Si-substituted hydrogarnets, Acta Mater. 55 (2007) 1183–1191.
[140] R.A. Howie, V.V. Ilyukhin, Crystal structure of rustumite, Nature 269 (1977) 231.
[141] L. Zhang, P. Fu, H. Yang, K. Yu, Z. Zhou, Crystal structure of scawtite, Chin. Sci. Bull. 37 (1992) 930–934.
[142] C.E. Tilley, Scawtite, a new mineral from Scawt Hill, Co. Antrim, Mineral. Mag. 22 (1930) 222–224.
[143] J. Murdoch, Scawtite from Crestmore, California, Am. Mineral. 40 (1955) 505–509.
[144] J.D.C. McConnell, A chemical, optical and X-ray study of scawtite from Ballycraigy, Larne, N. Ireland, Am. Mineral. 40 (1955) 510–514.
[145] D. McConnell, J. Murdoch, The crystal chemistry of scawtite, Am. Mineral. 43 (1958) 498–502.
[146] J.J. Pluth, J.V. Smith, The crystal structure of scawtite, $Ca_7(Si_6O_{18})(CO_3)22H_2O$, Acta Crystallogr. (B29) (1973) 73–80.
[147] R. Rinaldi, M. Sacerdoti, E. Passadlia, Strätlingite: crystal structure, chemistry, and a reexamination of its polytype vertumnite, Eur. J. Mineral. 2 (1990) 841–849.
[148] W. Gessner, D. Müller, Solid-state NMR investigations of gehlenite hydrate $2CaO{\times}Al_2O_3{\times}SiO_2{\times}8H_2O$, Z. Chem. 29 (1989) 344–345.
[149] S. Kwan, J. Larosa, M.W. Grutzeck, Si-29 and Al-27 MAS NMR study of strätlingite, J. Am. Ceram. Soc. 78 (1995) 1921–1926.
[150] M. Frias, J.G. Cabrera, Influence of MK on the reaction kinetics in MK/lime and MK-blended cement systems at 20 °C, Cem. Concr. Res. 31 (2001) 519–527.
[151] A. Setiadi, N.B. Milestone, J. Hill, M. Hayes, Corrosion of aluminium and magnesium in BFS composite cements, Adv. Appl. Ceram. 105 (2006) 191–196.

[152] M. Frias, The effect of metakaolin on the reaction products and microporosity in blended cement pastes submitted to long hydration time and high curing temperature, Cem. Concr. Res. 36 (2006) 1–6.
[153] H.F.W. Taylor, D.M. Roy, Structure and composition of hydrates, Principal Report, Sub-Theme II-2, Proc. 7th Int. Cong. Chem. Cem., Paris, I, Editions Septima, Paris, 1980, II-2/1-II-2/13.
[154] H.F.W. Taylor, Crystal structures and properties of cement hydration products (calcium silicate hydrates), Proc. 5th Int. Symp. Chem. Cem., Tokyo, 2 (1968) 1–26.
[155] I.G. Richardson, The nature of C-S-H in hardened cements, Cem. Concr. Res. 29 (1999) 1131–1147.
[156] A.V. Girão, I.G. Richardson, C.B. Porteneuve, R.M.D. Brydson, Composition, morphology and nanostructure of C-S-H in white Portland cement-fly ash blends hydrated at 85 °C, Adv. Appl. Ceram. 106 (2007) 283–293.
[157] I.G. Richardson, A.R. Brough, R.M.D. Brydson, G.W. Groves, C.M. Dobson, The location of aluminium in substituted calcium silicate hydrate (C-S-H) gels as determined by $^{29}$Si and $^{27}$Al NMR and EELS, J. Am. Ceram. Soc. 76 (1993) 2285–2288.
[158] M.D. Andersen, H.J. Jakobsen, J. Skibsted, Incorporation of aluminum in the calcium silicate hydrate (C-S-H) of hydrated Portland cements: a high-field Al-27 and Si-29 MAS NMR Investigation, Inorg. Chem. 42 (2003) 2280–2287.
[159] G.K. Sun, J.F. Young, R.J. Kirkpatrick, The role of Al in C-S-H: NMR, XRD, and compositional results for precipitated samples, Cem. Concr. Res. 36 (2006) 18–29.
[160] S.A. Rodger, G.W. Groves, N.J. Clayden, C.M. Dobson, Hydration of tricalcium silicate followed by 29Si NMR with cross-polarization, J. Am. Ceram. Soc. 71 (2) (1988) 91–96.
[161] A.R. Brough, C.M. Dobson, I.G. Richardson, G.W. Groves, In situ solid-state NMR studies of $Ca_3SiO_5$: hydration at room temperature using $^{29}$Si enrichment, J. Mater. Sci. 29 (1994) 3926.
[162] I.G. Richardson, G.W. Groves, The structure of the calcium silicate hydrate phases present in hardened pastes of white Portland cement/blast-furnace slag blends, J. Mater. Sci. 32 (1997) 4793–4802.
[163] J.D. Bernal, J.W. Jeffery, H.F.W. Taylor, Crystallographic research on the hydration of Portland cement. A first report on investigations in progress, Mag. Concr. Res. 4 (11) (1952) 49–54.
[164] J.D. Bernal, The structure of cement hydration compounds, Proc. 3rd Int. Symp. Chem. Cem., London, 1952, Cement and Concrete Association, London, 1954, pp. 216–236.
[165] H.F.W. Taylor, J.W. Howison, Relationships between calcium silicates and clay minerals, Clay Miner. Bull. 3 (1956) 98–111.
[166] H.G. Kurczyk, H.E. Schwiete, Electronenmikroskopische und thermochemische Untersuchungen über die Hydratation der Calciumsilikate $3CaO{\cdot}SiO_2$ und β-$2CaO{\cdot}SiO_2$ und den Einfluß von Calciumchlorid und Gips auf den Hydratationsvorgang, Tonind.-Ztg. Keram. Rundsch. 84 (1960) 585–598.
[167] H.G. Kurczyk, H.E. Schwiete, Concerning the hydration products of $C_3S$ and β-$C_2S$, Proc 4th Int. Symp. Chem. Cem., vol. 1, 1962, pp. 349–358.
[168] D.L. Kantro, S. Brunauer, C.H. Weise, Development of surface in the hydration of calcium silicates. II. Extension of investigations to earlier and later stages of hydration, J. Phys. Chem. 66 (1962) 1804–1809.
[169] L.G. Shpynova, I.D. Nabitovich, N.V. Belov, Microstructure of alite cement stone (hydrated tricalcium silicate), Sov. Phys. Crystallogr. 11 (6) (1967) 747–751 (English translation of Krystallografiya).
[170] H. Stade, On the structure of ill-crystallized calcium hydrogen silicates.II. A phase consisting of poly-and disilicate, Z. Anorg. Allg. Chem. 470 (1980) 69–83 (in German).
[171] H. Stade, W. Wieker, On the structure of ill-crystallized calcium hydrogen silicates. I. Formation and properties of an ill-crystallized calcium hydrogen disilicate phase, Z. Anorg. Allg. Chem. 466 (1980) 55–70 (in German).
[172] H. Stade, W. Wieker, G. Garzo, On the structure of ill-crystallized calcium hydrogen silicates. IV. Anion composition of the hydration products of tricalcium silicate, Z. Anorg. Allg. Chem. 500 (1983) 123–131.
[173] H. Stade, D. Müller, G. Scheler, On the structure of ill-crystallized calcium hydrogen silicates. V. Studies on the coordination of Al in CSH (di,poly) by 27Al NMR spectroscopy, Z. Anorg. Allg. Chem. 510 (1984) 16–24.
[174] H. Stade, A.-R. Grimmer, G. Engelhardt, M. Magi, E. Lipmaa, On the structure of ill-crystallized calcium hydrogen silicates. VII. Solid state silicon-29 NMR studies on C-S-H (Di,Poly), Z. Anorg. Allg. Chem. 528 (1985) 147–151 (in German).
[175] H. Stade, D. Müller, On the coordination of Al in ill-crystallized C-SH phases formed by hydration of tricalcium silicate and by precipitation reactions at ambient temperature, Cem. Concr. Res. 17 (1987) 553–561.
[176] Å. Grudemo, The crystal structures of cement hydration—A review and a new gel structure model, CBI (Cement och Betong Institutet [Swedish Cement and Concrete Research Institute]) Report ra 1 86 (1986) 3 –16. (Reprinted from Nordic Concrete Research, 1984).
[177] H.F.W. Taylor, Proposed structure for calcium silicate hydrate gel, J. Am. Ceram. Soc. 69 (6) (1986) 464–467.
[178] F.P. Glasser, E.E. Lachowski, D.E. Macphee, Compositional model for calcium silicate hydrate (C-S-H) gels, their solubilities and free energies of formation, J. Am. Ceram. Soc. 70 (7) (1987) 481–485.
[179] I.G. Richardson, G.W. Groves, Models for the composition and structure of calcium silicate hydrate (C-S-H) gel in hardened tricalcium silicate pastes, Cem. Concr. Res. 22 (1992) 1001–1010.
[180] I.G. Richardson, G.W. Groves, The incorporation of minor and trace elements into calcium silicate hydrate (C-S-H) gel in hardened cement pastes, Cem. Concr. Res. 23 (1993) 131–138.
[181] H.F.W. Taylor, Nanostructure of C-S-H: current status, Adv. Cem. Based Mater. 1 (1993) 38–46.
[182] X. Cong, R.J. Kirkpatrick, $^{29}$Si MAS NMR study of the structure of calcium silicate hydrate, Adv. Cem. Based Mater. 3 (1996) 144–156.
[183] X. Cong, R.J. Kirkpatrick, $^{17}$O MAS NMR investigation of the structure of calcium silicate hydrate gel, J. Am. Ceram. Soc. 79 (1996) 1585–1592.
[184] M.W. Grutzeck, A new model for the formation of calcium silicate hydrate (C-S-H), Mater. Res. Innov. 3 (1999) 160–170.
[185] M.W. Grutzeck, S. Kwan, J.L. Thompson, A. Benesi, A sorosilicate model for calcium silicate hydrate (C-S-H), J. Mater. Sci. Lett. 18 (1999) 217–220.
[186] A. Nonat, X. Lecoq, The structure, stoichiometry and properties of CS-H prepared by $C_3S$ hydration under controlled conditions, in: P. Grimmer, A.-R. Grimmer, H. Zanni, P. Sozzani (Eds.), Nuclear Magnetic Resonance Spectroscopy of Cement-Based Materials, Springer, Berlin, 1998, pp. 197–207.
[187] J.J. Chen, J.J. Thomas, H.F.W. Taylor, H.M. Jennings, Solubility and structure of calcium silicate hydrate, Cem. Concr. Res. 34 (2004) 1499–1519.
[188] A. Nonat, The structure and stoichiometry of C-S-H, Cem. Concr. Res. 34 (2004) 1521–1528.
[189] I.G. Richardson, Tobermorite/jennite-and tobermorite/calcium hydroxide-based models for the structure of C-S-H: applicability to hardened pastes of tricalcium silicate, beta-dicalcium silicate, Portland cement, and blends of Portland cement with blast-furnace slag, metakaolin, or silica fume, Cem. Concr. Res. 34 (2004) 1733–1777.
[190] K. Garbev, P. Stemmermann, L. Black, C. Breen, J. Yarwood, B. Gasharova, Structural features of C-S-H(I) and its Carbonation in air— a Raman spectroscopic study. Part I: Fresh phases, J. Am. Ceram. Soc. 90 (2007) 900–907.
[191] C.A. Love, I.G. Richardson, A.R. Brough, Composition and structure of C-S-H in white Portland cement-20% metakaolin pastes hydrated at 25 ° C, Cem. Concr. Res. 37 (2007) 109–117.
[192] A.V. Girão, I.G. Richardson, C.B. Porteneuve, R.M.D. Brydson, Composition, morphology and nanostructure of C-S-H in white Portland cement pastes hydrated at 55 ·C, Cem. Concr. Res. 37 (2007) 1571–1582.
[193] R. Taylor, I.G. Richardson, R.M.D. Brydson, Nature of C-S-H in 20 year old neat ordinary Portland cement and 10% Portland cement—90% ground granulated blast furnace slag pastes, Adv. Appl. Ceram. 106 (2007) 294–301.

[194] I.G. Richardson, Electron microscopy of cements, in: P. Barnes, J. Bensted (Eds.), Chapter 22 in Structure and Performance of Cements, 2nd ed., Spon Press, London, 2002, pp. 500–556.
[195] I.G. Richardson, G.W. Groves, The microstructure and microanalysis of hardened cement pastes involving ground granulated blast-furnace slag, J. Mater. Sci. 27 (1992) 6204–6212.
[196] I.G. Richardson, G.W. Groves, The composition and structure of C-S-H gels in cement pastes containing blast-furnace slags, Proc. 9th Int. Cong. Chem. Cem., New Delhi, IV, 1992, pp. 350–356.
[197] I.G. Richardson, G.W. Groves, The microstructure and microanalysis of hardened ordinary Portland cement pastes, J. Mat. Sci. 28 (1993) 265–277.
[198] I.G. Richardson, A.R. Brough, G.W. Groves, C.M. Dobson, The characterization of hardened alkali-activated blast-furnace slag pastes and the nature of the calcium silicate hydrate (C-S-H) phase, Cem. Concr. Res. 24 (1994) 813–829.
[199] I.G. Richardson, The structure of C-S-H in hardened slag cement pastes, Proc. 10th Int. Cong. Chem. Cem., Göteborg, vol. 2, 1997, 2ii068, 8pp.
[200] I.G. Richardson, The nature of the hydration products in hardened cement pastes, Cem. Concr. Compos. 22 (2000) 97–113.